Short Range Millimeter-Wave Inverse Synthetic Aperture Radar Imaging

OSCAR GYLLING
RICKARD STÅHL
MASTER´S THESIS
DEPARTMENT OF ELECTRICAL AND INFORMATION TECHNOLOGY
FACULTY OF ENGINEERING | LTH | LUND UNIVERSITY

Short Range Millimeter-Wave Inverse Synthetic Aperture Radar Imaging

Oscar Gylling & Rickard Ståhl

Department of Electrical and Information Technology
Lund University

Supervisors: Lars Ohlsson & Sebastian Heunisch

Examiner: Mats Gustafsson

June 19, 2018

Printed in Sweden
Tryckeriet i E-huset, Lund

Abstract

Millimeter-wave radar imaging has potential uses in applications such as material analysis and medical in-vivo scanning of tissue. This thesis is about measuring objects using a millimeter wave radar, implement radar imaging algorithms and evaluate the resulting images. The measured objects are plates and rods made of metal and a rod made of acrylic glass (PMMA). The objects are measured using the inverse synthetic aperture radar technique, in which the radar is stationary and and the scene is either moving in a line or rotating in front of the radar, in our case at a few decimeters distance. A pulse generating circuit is used as transmitter and the receiver is a sampling oscilloscope. Multiple imaging algorithms, including backprojection and gridding, are implemented in Matlab. In order to test the algorithms, scripts are implemented to create simulated ideal data from line and rotation measurements. Data for multiple point scatterers is simulated and used in the imaging algorithms to identify if the scatterers are correctly resolved. Using this approach the implemented methods are shown to work as intended. Using strip-map measurement data for two separated metal plates it is shown that an image can be produced where the objects are resolved with correct width, spacing and down-range position. Both the backprojection and gridding algorithms are shown to produce higher quality images with a resolution of less than one centimeter when used in spotlight mode. For gridding it is found that objects with a small distance-to-radius ratio are distorted, which limits the object size for a specific distance.

Popular Science Summary

While radars previously mostly have been used in military and aviation, development of smaller cheaper radars in recent years has lead to a high interest for using radars as an alternative to other sensors such as IR-sensors and cameras. Some new areas where radars are being tested are mapping the surroundings of self driving cars to avoid collisions, high resolution imaging, material analysis and gesture recognition to allow control of computers simply by making hand gestures in front of it. Another useful application of radars is medical scanning of tissue. This technique could for example be used to detect skin cancer.

In this thesis we have investigated how high quality images of objects can be created using a radar. To create an image we need to fill the pixels in the image with information from different points in space. This information needs to be gathered with some kind of sensor. If we take the example of a camera, it has many light sensitive sensors side by side and the information in each of these sensors is later displayed as a unique pixel. Most radars only work as a single sensor and gather information from a large area in front of it. To be able to create an image, a technique called synthetic aperture radar is used. In this method the radar scans a certain area in space. The data from all the different antenna positions can then be combined to create an artificial sensor matrix similar to that in a camera. After processing, the data then corresponds to unique pixels in the image.

The benefit of using radar to create images is that they can see through materials that cameras can not, for example smoke and fog but also solid materials like soil can be penetrated. Since the radar transmits its own signal it does not require external light like a camera does. Furthermore, the range to objects can be calculated.

In this thesis two different methods for converting measurement data into images were implemented and tested. The first one is called backprojection and is a time domain method, which means that processing is done on the measured time dependent signal. The positions of the radar and object for different measurements are considered and combined to produce an image. The other method is called gridding, in which the measured signal is first transformed into the frequency domain. A frequency domain signal is described by what frequencies build up the signal, rather than a time domain signal in which the signal level at different times is described. The image is produced by rearranging the data in the frequency

domain according to the measurement geometry and then returning to the time domain (or spatial domain).

With these two methods we were able to produce images with high resolution. We also learned what the different limitations of the two methods were. The backprojection is slow but achieves the best images, while also being flexible since it works for any measurement data. The gridding method is faster but it has certain criteria of the measurement setup, for example the distance to the object needs to be large compared to its size.

Acknowledgements

We would like to thank our supervisors Sebastian Heunisch and Lars Ohlsson for the good discussions and guidance that they have provided during our thesis. Also, we really appreciate the help from Sebastian with planning and setting up the lab and measurements.

Table of Contents

List of Figures

Chapter 1
Introduction

Radar was originally an acronym for radio detection and ranging that was made in the 1940s [18, 3], but has since become a noun. Radar is a system used to detect distant objects using electromagnetic waves. Depending on type of radar and the intended purpose, a radar can be used to determine range, angle or velocity of the objects. In order to get information about a target, a radar needs a transmitter that usually transmits in the radio or microwave bands (a few hundred MHz to hundreds of GHz) [2]. The transmitted waves interact with objects, inducing currents in the target surface. These currents produce new electromagnetic waves that radiate outwards. A portion of these scattered waves return and are detected by a receiver [6]. Using a signal processor the received signal can then be processed to obtain information about the object.

Modern uses of radars are found in many areas, for example air traffic control, radar astronomy, marine radars and flight control systems [19, p. 2]. Millimeter-wave radars can be used for mapping the surroundings of self driving cars to avoid collisions and for gesture recognition, which could be used to control computers. Material analysis can also be done, for example radars can be used for medical imaging of tissue. An important application for radars is to collect data of remote objects that can then be used to produce images. This is often done by collecting radar signals from multiple angles or positions around a target scene, a method called synthetic aperture radar (SAR) [9]. However, it is also possible to have a stationary radar system and move or rotate the target scene instead, a technique called inverse-SAR (ISAR) [12, p. 121]. Through signal processing, the collected data can be turned into an image by combining the collected data from several angles or positions. The image quality and contents will depend on the type of measurement and the properties of the radar. The benefit of using radars to create images is that they can see through materials that optical cameras can not, for example smoke and fog but also solid materials like soil can be penetrated. They can also be used to identify materials properties such as permittivity [3]. Possible applications include biomedical scanners to analyze skin tissue for cancer, which have been shown to contain a higher water content than regular tissue [11]. Radars are also used as body scanners for airport security, where a detailed mapping of metal objects could be obtained as opposed to a conventional metal detector that only alerts if any metal is detected.

The aim of this thesis was to investigate an in-house radar transmitter ([10]) and see whether it is possible to use it to create high quality ISAR images. We

planned and then conducted radar measurements on various objects of different materials. Using the signal data recorded in time domain by an oscilloscope the main focus was to process the data in Matlab and implementing algorithms for ISAR imaging. We would primarily focus on producing images of conducting objects made of metal and see if we can identify the size, shape and fine details of the objects in the produced images. We would also investigate the performance and resolution of different ISAR methods and evaluate their limitations.

Following this introduction, the remainder of this thesis is structured as follows. In Chapter 2 - "Theory", we describe the theory required to understand radars, radar imaging and signal processing. Chapter 3 - "Radar and Measurement Setup", contains the radar setup and different ISAR measurements, with separate sections for strip-map and spotlight. In Chapter 4 "Imaging", a detailed explanation of the imaging algorithms and implemented methods is given as well as methods for generating simulated data. In chapter 5 - "Results and Discussion" we present the final radar ISAR images using the different implemented methods. We also evaluate the measurements and algorithms, discuss problems and possible improvements. Chapter 6 - "Conclusions and Outlook" is a summary of the thesis with suggested future applications. In the appendix "Matlab code", the scripts for the simulations and imaging methods are added.

Chapter 2
Theory

This chapter introduces the theory of radar imaging and signal processing used in this thesis.

2.1 Fundamentals of Electromagnetism

Electromagnetic (EM) waves radiate from charged particles when they are accelerated [21, p. 21]. When an electron is stationary or moving with a constant velocity, an electric field will always point in the radial direction of the electron. If the electron is accelerated an electric field orthogonal to the radial electric field will be created during the time of acceleration and propagate in the radial direction with the speed of light c, Figure 2.1. At the same time a magnetic field orthogonal to both the electric field and the direction of propagation will also be created. In Figure 2.1 an electron is first stationary, with the radial field E_0. It is then

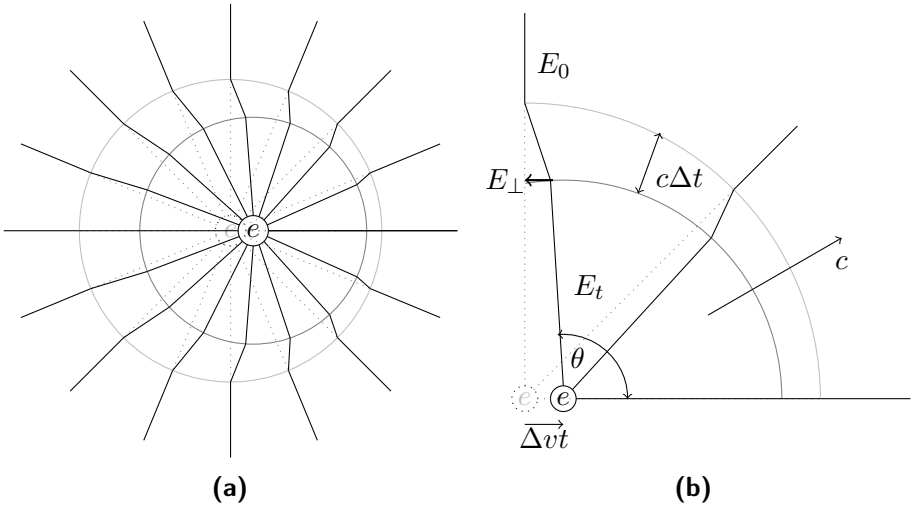

Figure 2.1: An electron being accelerated, resulting in the propagation of an electric field $E_\perp$ orthogonal to E_0 and E_t far ways from the electron.

accelerated to a velocity Δv during a time Δt. Traveling at a constant velocity Δv after the acceleration the electron creates the electric field E_t. The new field E_t propagates outwards with the speed of light. Far away from the electron the previous field E_0 still exists and remains unchanged. Between E_0 and E_t there is a region with the extent $c\Delta t$ caused by the acceleration. Since the electric field need to be continuous the region $c\Delta t$ must contain a non-radial field component $E_\perp$, orthogonal to the radial electric field. While the radial electric field strength decreases as $\frac{1}{r^2}$, where r is the distance from the electron, the orthogonal field only decreases as $\frac{1}{r}$ [21, pp. 21-23]. A similar derivation can be done for the magnetic field that will show that where $E_\perp$ exists, there will also exist a magnetic field $B_\perp$ orthogonal to $E_\perp$ and the direction of propagation. The propagating waves in the electric field $E_\perp$ and the magnetic field $B_\perp$ is the electromagnetic radiation.

2.2 Scattering

An electromagnetic wave that propagates in space will interact with objects it encounters. The charges in an object hit by the electromagnetic wave will be accelerated by the electric field component and in turn emit their own radiation. This phenomenon is called scattering.

In perfect electric conductor (PEC) materials such as metal, a good model is that the incident field induces currents in the surface of the bulk, which then re-radiate an electromagnetic field. However, non-conducting materials such as plastic can also scatter. The bound charges in the materials will start to oscillate and in turn radiate a new field. Compared to a PEC, only a portion of the field will radiate back at the first interface between materials, while the rest of the wave continues into the bulk. The amount of scattering is related to the difference in permittivity in an interface (for example between air and plastic). PECs can be seen as having infinite permittivity as no field enters the bulk [1].

Scattering can be categorized by comparing the wavelength of the EM wave to the size of the object features, see figure 2.2. When the wavelength is much

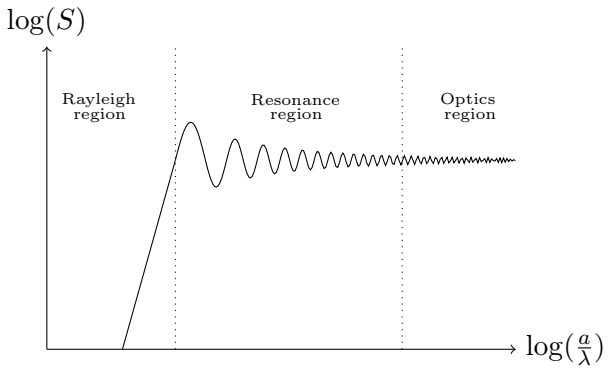

Figure 2.2: How the scattering amplitude changes for a sphere, when the ratio of diameter a to wavelength λ increases [18, p.174].

longer than the object features, it is called Rayleigh scattering. The amount of scattering S in this region is exponentially dependent of the wavelength. When the wavelength is much shorter than the object features, it is called specular scattering (optics region in Figure 2.2). The electromagnetic wave is reflected in a similar way to visible light and is almost independent of wavelength. Between these two regions, there is a resonance region where the scattered amplitude varies periodically [27]. In this region the object feature size is similar to the wavelength.

In the optical region a simple model is that objects are built up of point scatterers, which can be seen as infinitely small points that scatter electromagnetic waves isotropically. Adding the EM waves from all point scatters, the far field will be an interference pattern, following that the point scatterers have different phases. The electric field for one point in a plane can be described by

$$E(k,\theta) = \sum_{n=1}^{N} A_n e^{-i2\vec{k}\vec{r_n}} \tag{2.1}$$

where E is the electric field in a point defined by the spatial frequency k and angle θ, n is the point scatterers, A_n is the complex amplitude for scatterer n and $\vec{r_n}$ is the distance from the point scatterer to the point where E is measured [12, p. 273]. In real applications the polarization of $E(k,\theta)$ would also need to be taken into account.

2.3 Basic Radar Principles

Radars operate by transmitting electromagnetic radiation with a transmitter toward a region and detecting the scattering from objects within this region with a receiver. The received signal is then processed with a signal processor to obtain information about the target's range, angle and speed. Figure 2.3 shows the basic principle and relevant elements of a radar system. The transmitter and receiver

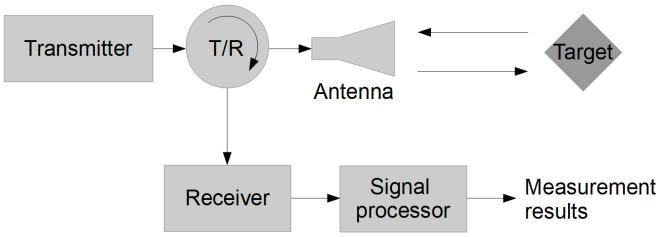

Figure 2.3: Radar principle and the basic required elements. The T/R block is a duplexer which allows transmitted signals to only pass to the antenna and received signals to only pass to the receiver.

usually use the same antenna, similar to in Figure 2.3, in which case the radar is called monostatic. A bistatic radar has separate antennas for transmitter and receiver. If two individual antennas are close to each other as compared to the

distance between target and receiver and they are pointing in the same direction, the radar is considered to be quasi-monostatic [13, p. 109].

2.3.1 Power Transmission

Consider a one way transmission between two antennas separated by a distance, d. Assuming free space propagation with matched polarization between the transmitting and receiving antennas, the received power

$$P_r = P_t G_t G_r \left(\frac{\lambda}{4\pi d}\right)^2, \tag{2.2}$$

where P_t is the transmitted power, G_t and G_r are the transmitter and receiver antenna realized gain respectively (which includes losses due to impedance mismatch at antenna ports) and λ is the free-space wavelength [15, p. 4].

For a radar, the transmitted signal first needs to reach an object, which then needs to scatter a portion of the signal back to the radar. A commonly used concept is the radar cross section (RCS) denoted by σ, which is a measure comparing the EM energy intercepted and reradiated by an object. The unit of RCS is m^2 and it is dependent of the object's shape, what angle the wave intercepts and scatter, as well as the frequency and polarization of the wave. RCS is defined as

$$\sigma = \lim_{R\to\infty} \left(4\pi R^2 \frac{W^s}{W^i}\right), \tag{2.3}$$

where R is the distance from radar to the object, W^i is the incident power density on the object and W^s is the power density of the reflected wave [12, pp. 37-39]. For a monostatic radar, the received power from a target is described by the radar range equation

$$P_r = \frac{P_t G_t G_r \lambda^2 \sigma}{(4\pi)^3 R^4}. \tag{2.4}$$

The R^4 comes from the fact that the power decreases by the square of the distance for a one way transmission (the field radiates in a sphere) and the same is true for the scattered field, of which a portion returns to the radar [18, p. 64].

2.3.2 Signal-To-Noise Ratio

The received radar signal contains noise which originates from various sources such as from the atmosphere and thermally agitated random motion of electrons in the receiver (thermal noise). The signal-to-noise ratio (SNR) can be approximated using

$$\mathrm{SNR} = \frac{P_t G_t G_r \lambda^2 \sigma}{(4\pi)^3 R^4 k T_0 F L_s}, \tag{2.5}$$

where k is Boltzmann's constant, T_0 is room temperature, F is the noise figure and L_s is losses (such as transmit, receiver, atmospheric and signal processing losses) [18, pp. 67-68].

2.3.3 Waveforms

A radar signal can either be transmitted as a continuous wave (CW) or as pulses. For each type of signal the carrier frequency can be kept constant but it can also be modulated, such as in frequency modulated continuous wave (FMCW) radars and chirped pulse radars. Assuming free space, a transmitted wave will propagate at the speed of light c and the total travel time from transmitter to receiver will be equivalent to two times the distance to the target multiplied by c. From a received radar signal the distance R to the target can thus be calculated as

$$R = \frac{c\Delta T}{2}, \tag{2.6}$$

where ΔT is the time between transmission and the reflected signal being received. For a radar using a single carrier frequency, it is only possible to measure distance to a target using pulses (assuming the distance is larger than the wavelength). In a pulsed radar each pulse has a defined time at which it is transmitted and received, which is a requirement to obtain ΔT. For a continuous wave, there is no way to determine when the instantaneous received signal was transmitted, which means that ΔT is unknown. However, if the wave has a changing frequency as in FMCW, the instantaneous transmitted and received frequencies can be compared and the distance calculated from the rate at which the frequency is modulated. The frequency is usually swept in a ramp, with either a triangular or sawtooth wave, from f_{min} to f_{max} [12, pp. 54-57].

The waveforms of a pulsed radar signal in time domain and the control signal which generates the pulse is shown in Figure 2.4. Note that depending on what circuit is used the RF signals do not always necessarily begin with the same phase. The pulse repetition interval (PRI) determines the unambiguous range R_{ua}

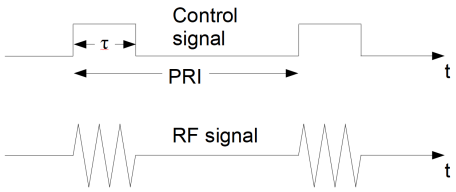

Figure 2.4: Pulsed radar signal in time domain and corresponding control signal to generate the pulses.

(Equation 2.7), which is the longest distance a target can be from the radar and still be detected at the correct range.

$$R_{ua} = \frac{c}{2}PRI \tag{2.7}$$

Returns from targets beyond this limit will be received after the waiting time for a pulse has passed. It will thus be interpreted by the radar as a return from one of the next transmitted pulses, and the calculated distance will thus be false. In essence, a target must be close enough for the echo to return before the next pulse

is transmitted. The ambiguous range can be increased by increasing PRI but that will also reduce the pulse repetition frequency (PRF=1/PRI), which sets the radar data collection rate.

2.3.4 Attenuation

EM-waves are attenuated as they pass through the atmosphere. Two processes are involved: absorption and scattering. Absorption is a mechanism in which some of the EM-waves energy is lost as heat to gas molecules or particles such as rain drops. The losses are heavily dependent on the wavelength. For example, there is a 17 dB/km O_2 absorption peak at 60 GHz. Scattering is when larger particles cause a portion of the wave to change direction and thus the power in the original direction decreases [18, pp. 121].

Attenuation is not always an unwanted mechanism. For example, a frequency for a short range radar can deliberately be chosen so that the radar attenuation in air is high. This enables many users to operate the same type of radar, using the same frequency, without interfering each other. For radar imaging at close range high attenuation is advantageous since it reduces clutter from objects in the background beyond the scene of interest.

2.4 Synthetic Aperture Radar

Synthetic aperture radar (SAR) is a high-resolution remote sensing and imaging technique for targets in a stationary scene. By collecting echo signals from more than one position a large synthetic aperture can be created. The effect is the same as having a single physically large antenna aperture. SAR has some key advantages over optical photography. It can be used during night time, in weather opaque for visible light. This is advantageous for meteorology and military applications. Radar signals with low frequency can penetrate foliage and even the ground [18, p. 836]. This can be used for applications in geophysics, and archeology [12, p. 79]. Millimeter wave radar imaging could be suitable for medical scanning of tissue. This technique could for example be used to detect skin cancer [8]. Radar signals are coherent, which means that the carrier phase is known. This leads to additional information since each pixel of a SAR image will have complex values as compared to optical photography where only light intensity is measured.

In order to obtain range information, the echo delay of a transmitted signal must be known. This is possible when using FMCW or pulsed radars, however continuous CW can not be used.

While SAR specifically refers to the case when the target scene is stationary while the radar is moving, inverse-SAR (ISAR) is when the target is moving while the radar remains stationary. An example is imaging of airplanes and ships. ISAR is also advantageous when it is impractical to move or rotate the radar.

2.4.1 ISAR Modes

ISAR (and SAR) can be divided into different modes depending on how the scanning is operated. There are two main modes: strip-map and spotlight.

Strip-map is a measuring technique where the scene of interest is moving in a line in front of the radar, see Figure 2.5. Multiple measurements are done at

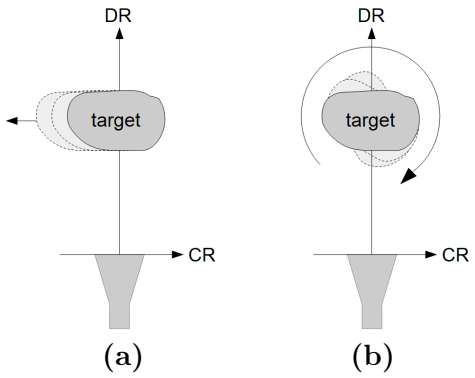

Figure 2.5: ISAR modes. DR is down-range and CR is cross-range. (a) strip-map. (b) spotlight.

different locations, giving a dataset of measurements mapping the scene. The data matrix has one dimension with a time quantity called fast time. This is the time difference between transmitting a signal and receiving it. Fast time can be recalculated to range (total distance) using Equation 2.6. The direction parallel to the radar beam is referred to as down-range. The sideways direction as seen from the radar antenna is called cross-range (perpendicular to down-range). This is determined by the position of the object relative to the antenna as it moves and is the quantity of the other dimension of the data matrix.

In spotlight mode, the scene is rotating in front of the radar. This means that the measured data matrix has an angular dependence rather than a positional one. The benefit of this technique is that the object is kept within the antenna's main beam at all times, which leads to a higher signal strength since the antenna gain is always maximum. In strip-map the object is swept past the antenna and is only directly in front of the antenna at one of the positions.

2.4.2 Resolution

When referring to resolution in SAR it is usually divided into down- and cross-range resolutions. High down-range resolution Δy is obtained by having a wide bandwidth transmitted signal, according to

$$\Delta y = \frac{c}{2B} \tag{2.8}$$

where B is the bandwidth [18, p. 845]. For FMCW this is typically achieved by having a large frequency span between f_{min} and f_{max}. For a single frequency pulsed radar an estimate of the bandwidth of one pulse is

$$B = 2/\tau \tag{2.9}$$

where τ is the pulse width. Therefore, the resolution can be increased by having shorter pulses. However, shorter pulses also means that less energy is emitted per pulse, which reduces the total power per pulse repetition interval (PRI). This in turn reduces the SNR according to Equation 2.5. The optimum pulse to achieve both high SNR and high resolution would be as short as possible and have as high power as possible, the ideal being a Dirac delta function. Since this is not possible in practice a trade-off between SNR and resolution has to be made. Note that the pulse bandwidth can also be defined in other ways, such as a width of the main lobe of the pulse signal in the frequency domain. Ways to improve the down-range resolution includes pulse compression techniques such as using chirped pulses. In such a radar, the frequency within each pulse is ramped from a lower to a higher frequency (or vice versa). This results in a higher bandwidth and thus better resolution, without the need to make the pulses shorter. Additionally, being able to have a longer pulse means that the average power is higher and thus also the SNR according to Equation 2.5. [4]

The cross-range resolution, Δx, depends on the measurement mode. For strip-map it is equal to

$$\Delta x = \frac{\lambda}{2 \sin \Phi} \tag{2.10}$$

where Φ is the illumination angle, as seen in Figure 2.6 [15, p. 43]. For a 360

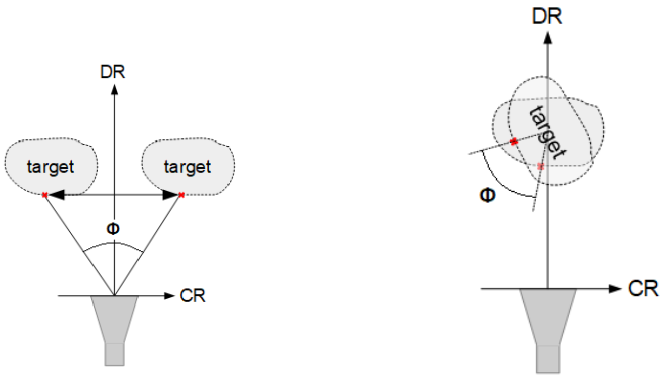

Figure 2.6: Definition of the illumination angle Φ for ISAR measurements [19, p. 9]. Each figure shows the start and end position of the scan. The red dots represent the same point on the object. (a) Strip-map. (b) Spotlight.

degree spotlight measurement, the cross-range resolution is equal to the down-range resolution in Equation 2.8 [15, p. 43]. This is because the scene is viewed in down-range from all angles.

2.5 Signal Processing

In order to extract information from the measured data signal processing is generally needed. Here we discuss some relevant concepts used in signal processing.

2.5.1 Discrete Fourier transform

Fourier transform is a mathematical tool that allows an easy transformation between time and frequency domain [12, p. 2]. This makes it very useful when analyzing periodic signals. The continuous Fourier transform is defined as

$$G(f) = \int_{-\infty}^{\infty} g(t)e^{-i2\pi ft}dt, \tag{2.11}$$

where $G(f)$ is the signal in the frequency domain, $g(t)$ is the signal in the time domain and $e^{-i2\pi ft}$ is the function which $g(t)$ is projected on. In the continuous Fourier transform, at least one of the functions $G(f)$ or $g(t)$ has infinite support. When working with discrete signals some modification needs to be done to the continuous Fourier transform to still get a usable transformation.

A measured signal is not continuous but instead a series of samples taken at certain times from the continuous signal. The discrete signal, $s(nT)$, is described by

$$s(nT) = \int_{-\infty}^{\infty} s(t)\delta(t - nT)dt, \tag{2.12}$$

where $s(t)$ the continuous signal and T the time between samples. Inserting $s(nT)$ in the Fourier transform results in Equation 2.13. Since $s(nT)$ only exist for $n = \mathbb{Z}$, $e^{-i2\pi ft}$ can be rewritten as $e^{-i2\pi fnT}$.

$$G(f) = \sum_{n=-\infty}^{\infty} s(nT) \cdot e^{-i2\pi fnT} \tag{2.13}$$

$e^{-i2\pi fnT}$ is periodic with frequency $1/T$ which makes $G(f)$ repeat with the same frequency and the amplitude in one frequency bin is the sum of multiple frequencies since $e^{-i2\pi fnT}$ is only orthogonal up to $f = 1/T$. This phenomenon is called aliasing and is a problem if a signal is sampled too sparsely.

It should also be considered that a measured signal has a finite support, which would require the signal to have an infinite support in the frequency domain according to Benedicks's theorem [24]. If we assume that $s(nT)$ is periodic with N, the discrete Fourier transform (DFT) can now be expressed as

$$G(f) = \sum_{n=0}^{N-1} s(nT) \cdot e^{-i2\pi fnT/N}, \tag{2.14}$$

where $0 \leq n \leq (N - 1)$ is the support of $s(nT)$. The limited support can be seen as if a signal with infinite support is multiplied by a box function. This will lead to a convolution between $G(f)$ for the infinitively supported function and a sinc function that is the result of the box/finite support. This results in spectral leakage and reduces the resolution of the discrete Fourier transform.

The spectral leakage can be decreased by choosing a suitable window function. The window function will replace the box and weight the amplitude differently. To get less leakage to side lobes a more smooth function should be used since it will have less high frequency components and converge faster towards zero but have a wider main lobe due to more low frequency content.

When using computers, a version of the DFT called fast Fourier transform (FFT) is often used due to its fast computational speed [5, p. 6]. However, since an infinite number of data points is not possible in a computer, both time and frequency domain have a limited support and are discrete. Both sides being discrete will lead to some frequencies or times falling between bins and will lower the resolution.

2.5.2 Interpolation

If the data has been sampled sparse one would like to create new data points between the sampled points [5, p. 189]. These new points should estimate the value of the continuous signal as good as possible. To achieve this, some form of interpolation need to be done. Generally the values from sampled data points within a certain distance of the new point being created is weighted and added together. This can be described by a convolution between the signal and a weighting function $w(x)$. In the frequency domain the weighting function should be a low pass filter, only using the continuous wave functions with frequencies lower than half the sampling frequency to create new data points. If higher frequencies were used, aliasing would be introduced.

A common method is sinc interpolation, where the weighting function is a sinc [5, pp. 173-175]. If the original signal band limit is lower than half the sampling frequency, the signal can be perfectly reconstructed. The sinc function however has an infinite support and converges slowly towards zero. In a computer with finite vectors the sinc either needs to be cut to increase computational speed, which means losing a lot of information or the vector can be long and accurate but the computation will take a long time. To get a function that converges faster, a function that is smoother in the frequency domain need to be used. The Kaiser-Bessel window is a good alternative but since this function is not an ideal low pass filter aliasing will be introduced and the frequencies will be multiplied by a weight, the weight can easily be removed by a deconvolution. The aliasing need to be minimized by choosing the right shaping factor β for the Kaiser-Bessel window [26]

$$w(x) = \frac{I_0(\beta\sqrt{1-(\frac{x-N/2}{N/2})^2})}{I_0(\beta)} \tag{2.15}$$

$$\beta = \pi\sqrt{\frac{J^2}{(K/N)^2}(\frac{K}{N}-\frac{1}{2})^2 - 0.8}, \tag{2.16}$$

where $w(x)$ is the Kaiser-Bessel window, I_0 is the zeroth order modified Bessel function, N is the length of the window vector and β is the shape factor. In β, J is the width of windows support and K/N is the upsampling factor. This shape factor should minimize the aliasing according to [26].

2.5.3 Matched Filtering

Matched filtering is when a known signal, called a template, is compared to an unknown signal in order to look for the presence of the known signal in the unknown signal. This is usually done by cross correlating the two signals. It will return a high amplitude for a position in the unknown signal if this area has a large correlation with the template. It can be shown that the matched filtering maximizes SNR [12, p.86]. To detect a template $s(n)$ in an unknown signal $x(n)$ one would first create a filter $h(n) = Cs(k-n)$ and then use the matched filter

$$y(k) = \sum_{n=-\infty}^{\infty} h(k-n)x(n), \tag{2.17}$$

where y(k) is the cross correlation between $s(n)$ and $x(n)$.

Matched filtering can also be used for pulse compression, where a signal can be compressed in time by a ratio equal to its time-bandwidth product [12, p.101]. A pulse made from a single carrier frequency has a time bandwidth product of $T \cdot 1/T = 1$ and can thus not be compressed further by matched filtering.

Chapter 3
Radar Measurements

In this chapter the radar setup and ISAR measurements are described.

3.1 Radar Setup

3.1.1 Transmitter

The transmitter stage of the radar consists of an integrated RF circuit (from [10]) which is contacted in a probe station. A schematic view of the circuit can be seen in Figure 3.1. The design with an integrated resonant tunneling diode (RTD) in series

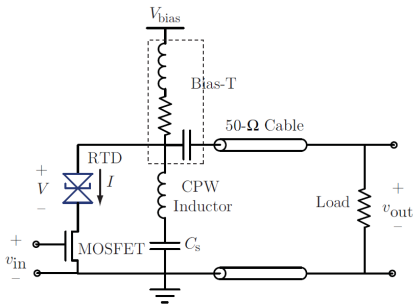

Figure 3.1: Radar transmitter circuit. Figure taken from [15, p. 18]

.

with a metal oxide semiconductor field effect transistor (MOSFET) allows for low power consumption during operation, since no power is consumed between each pulse transmission. This is in comparison to a conventional RF circuit which has a local oscillator running continuously when the device is powered on. The negative resistance provided by the RTD cancels out the positive load resistance and this makes the circuit oscillate when the loop is closed. The MOSFET is used to break the loop and thus controls pulse modulation, similar to Figure 2.4. An external signal generator is connected to the transistor gate via high frequency cables to the probe station. When v_{in} is high, the loop is closed and oscillation starts. Since the oscillation always starts with the same transient coherent signals can be generated. The pulse width, which should be short according to Equation 2.9, is

set to 80 ps (which is the shortest possible setting on the signal generator). The PRI is set to 10 ns, which means that the unambiguous range is 1.5 m according to Equation 2.7. The circuit frequency is set by the capacitance and inductance on the chip. It is between 60-65 GHz depending on what specific circuit is being used (there are many circuits on the same chip). Biasing is provided on the circuit output node by a voltage source through a bias-T. The bias-T allows DC current to pass to the circuit but not to the antennas, while allowing the high frequency AC currents to pass from the transmitter circuit to the antennas.

3.1.2 Leaky Lens Antennas

Two antennas are used in the setup, one for transmitting and one for receiving. These are positioned next to each other with a center-to-center spacing of 5.5 cm and pointing in the same direction. The transmitting antenna is connected through the bias-T to the transmitter, while the receiving antenna is connected to a sampling head of the receiver. The antennas are of a type called leaky lens antenna (from [15]). A thin leaky waveguide is used to maximize the field leakage. The field is then focused by a silicon hemisphere in front of the waveguide, which can be seen in Figure 3.2. The reason this type of antenna is used is that it is

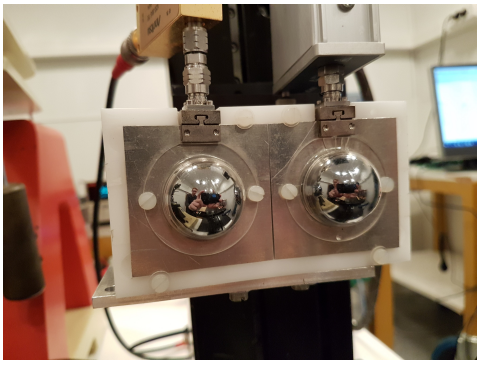

Figure 3.2: Leaky lens antennas. Left: transmitting antenna, with bias-T on top. Right: Receiving antenna, with sampling head on top.

suitable for a wide range of frequencies compared to most other types of antennas. As previously mentioned, the bandwidth of a pulse is inversely proportional to the pulse width τ. For this reason leaky lens antennas is a good choice to achieve high antenna gain when transmitting very short pulses. The low pulse distortion is beneficial for data analysis and imaging. The gain of the leaky lens antenna vs angle φ_t and frequency f is shown in Figure 3.3.

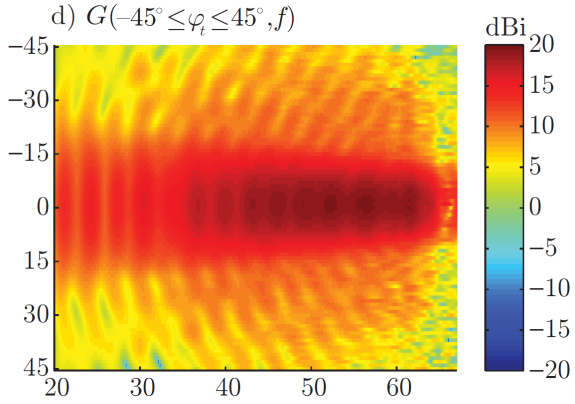

Figure 3.3: Leaky lens antenna gain vs frequency (f) and angle (φ_t). Figure taken from [15, p. 12]

3.1.3 Sampling Oscilloscope

The receiving stage of the radar setup is a LeCroy Wave Expert 100H oscilloscope. The maximum sampling frequency is below the carrier frequency of the transmitted signal. This is solved by using equivalent time sampling, where multiple pulse measurements are done with different trigger points to sample one pulse. This method allows for sampling up to the analog cut off frequency of the system (in this case limited by the cables to 70 GHz). The criteria is that the signal is repetitive and several pulses are required to sample one pulse.

In order to maximize the image quality the SNR should be high. This is done by averaging many pulses. For each ISAR measurement position or angle, a few thousand measurements are taken and the average is continuously calculated by the oscilloscope. Only the final averaged signal data is saved to the internal hard drive.

A clock sync cable is connected between the oscilloscope and signal generator. This is required for the oscilloscope to trigger correctly on each pulse and record time domain data. All instruments, including signal generator, voltage source, probe station and oscilloscope are connected to a common ground.

3.2 Measurement Setup

In this section the different types of measurement setups are explained. Detailed information about the parameters used for each specific measurement is described together with each final image in the "Results and discussion" chapter.

Before each measurement a reference pulse needs to be measured. This is done by placing a large (30 cm × 30 cm) metal plate in front of the antennas at a known distance, typically 20-30 cm, see Figure 3.4. The large plate provides a strong signal echo from transmitter to receiver. To ensure that the measured pulse is noise free the integration time is kept high (about 60 seconds). Figure 3.5 shows the time domain data for an averaged measured pulse from a reference plate. (a)

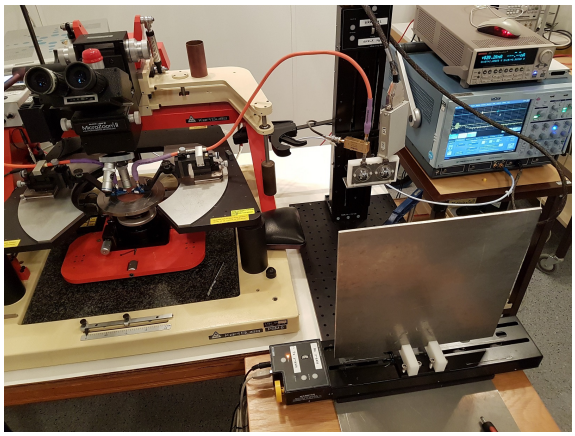

Figure 3.4: Measurement on a reference plate. Note that the plate is not moving in this measurement (the saved data is only for one position).

shows multiple reflections from the plate can be seen as pulses with decreasing amplitude after the first. The main pulse is zoomed in (b), where ringings from the circuit and bias-T can be seen after the pulse. The purpose of the reference

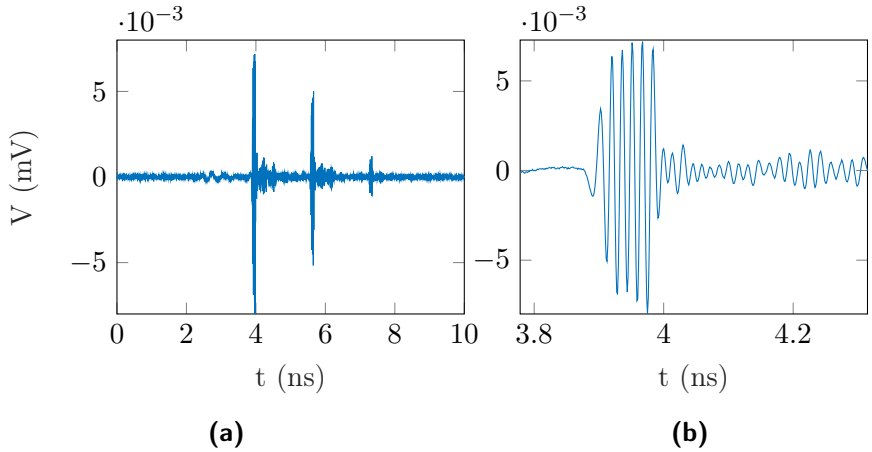

Figure 3.5: (a): Time domain data for a measured pulse from a reference plate. (b): Zoomed in on the main (first) pulse.

measurement is to obtain a pulse shape which will be used as a matched filter in the signal processing. Another use is to get a reference distance to be able to correctly set the scales of the final images. The reason that we can not extract the position from any measurement is that the position of the pulse in the fast time data does not represent an absolute distance. It is rather an arbitrary time on the oscilloscope window which is set manually before the recording starts. The recorded time domain data can only be used to compare a pulse position relative

to another pulse.

3.2.1 Strip-map

Strip-map measurements are done by using a linear actuator placed in front of the two radar antennas, on which various objects can be attached and be measured. Figure 3.6 shows an example of strip-map measurement setup. The actuator is

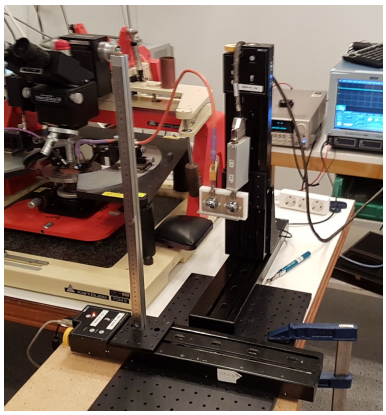

Figure 3.6: Strip-map measurement setup. The target object is attached on an actuator and can be moved in a line in front of the transmitter and receiver antennas.

controlled via a USB-connector to a computer, on which a Matlab script is used to set timings for when the actuator should move and what step size to use. The actuator can move the object up to 30 centimeters and the setup is chosen so that the object can move equal distances to the left and right of the center relative to the antennas.

Initially three measurements were done, two with flat metal strips of widths 3 and 6 cm (Figure 3.7 (a) and (b)) and one with a metal rod with a square profile, shown in Figure 3.6 from above in Figure 3.8. All objects extend in height beyond the vertical beam width of the antennas. This is not a problem considering the measurement is done in a horizontal line with zero elevation angle and there is no height information in the images anyway. Furthermore, the reflected signal will be larger from a long object compared to a short, which increases SNR.

Finally a measurement was done using multiple objects. Both the 3 and 6 cm metal strips were attached to the actuator, with a 2 cm spacing in down-range and 2.5 cm spacing in cross-range.

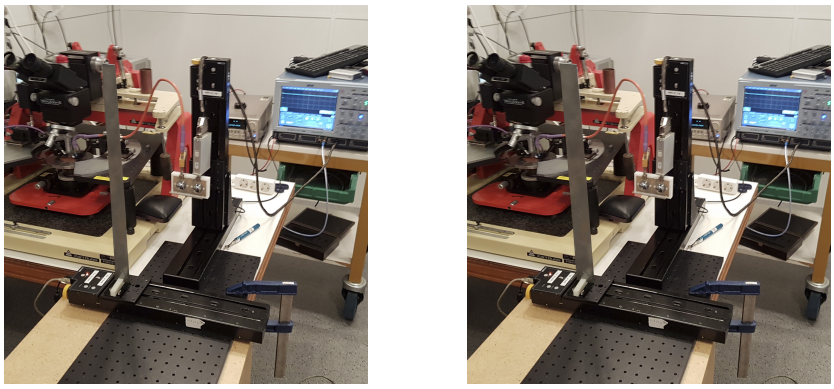

(a) (b)

Figure 3.7: Metal strips used in strip-map measurements. (a) 3 cm width. (b) 6 cm width.

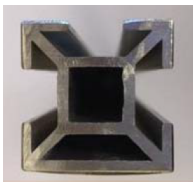

Figure 3.8: Metal profile used in measurements. The outer dimensions are 2 x 2 cm.

3.2.2 Spotlight

Spotlight measurements are done using a rotational actuator, as shown in Figure 3.9. Each measurement is done with a full 360 degree turn of the attached object, in steps of one or two degrees. The actuator is controlled by USB like the strip-map measurement and the oscilloscope takes a few thousand averages per position.

The first spotlight measurement used the metal profile pictured in 3.8 in 180 rotational steps. Another measurement was done using the metal profile and a acrylic glass (PMMA) rod on a rotating plate, as shown in Figure 3.9 (b).

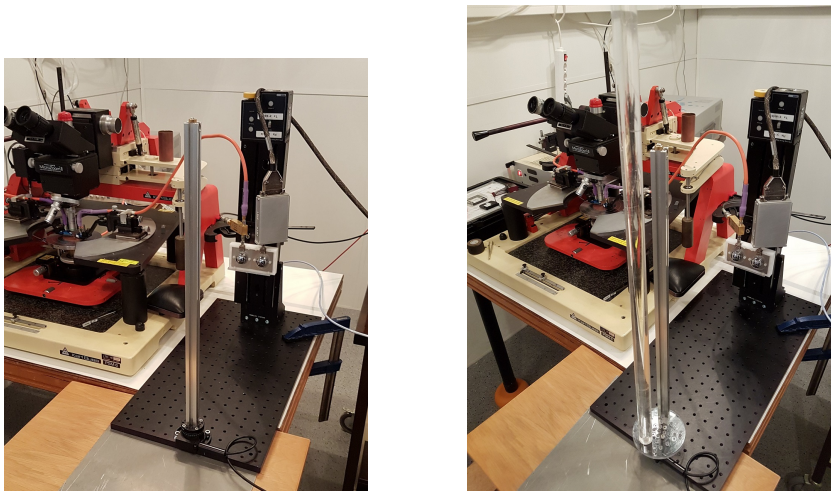

(a) **(b)**

Figure 3.9: (a): Spotlight measurement setup. The target object is attached on an actuator and can be rotated in front of the transmitter and receiver antennas. (b): Spotlight measurement using two objects attached on a plate on the actuator.

Chapter 4
Imaging

In this chapter each imaging algorithm is explained along with algorithms for generating simulated (ideal) data to test the algorithms. The Matlab implementations are also described and motivated. The code for each method is found in the appendix.

4.1 Algorithms

In this section the imaging algorithms for backprojection and gridding are explained.

4.1.1 Backprojection

A straight forward way to create an image from data consisting of radar measurements of an object at different positions or angles is called backprojection [17]. This is a method suitable for both strip-map and spotlight data. An important note is that while all measurements were done using ISAR, in the following backprojection algorithm the measurement setup is assumed to be in the SAR mode, in which the object is stationary while the antenna is moving in a line or in a circle around the object. This way of looking at the geometry is advantageous especially when making illustrations and describing the geometrical problem that is to be solved. Even if the implementation is made for the SAR case, it still works as intended for ISAR data since it is merely a change of perspective.

Assume that an object is placed in the (x, y) plane and radar measurements are taken for multiple antenna positions (x'_n, y'_n) in the plane, Figure 4.1. The recorded time domain data is on the form $E(t)$, where t is fast time. The data can be converted to $E(r)$, where r is the distance from antenna n at (x'_n, y'_n) to some point at (x, y) calculated from t using Equation 2.6. One data point $E(r)$ does not correspond to an exact position in the plane but instead all equidistant points r from the antenna, which can be seen as arcs in Figure 4.1, weighted by the antenna directivity $D(\theta)$ (it is assumed that the antennas always points towards the object). Multiple point scatterers S_i can be in the same range bin and contribute to the amplitude in one data point. Assume all point scatterers

contribute with the same amplitude, one data point P can be described by

$$P(E(r), x'_n, y'_n) \propto \oint_R D(\theta) S_i \tag{4.1}$$

where $P(E(r), \vec{a_n})$ is the data received at distance r from antenna a_n, $D(\theta)$ is the directivity of the antenna at different directions θ, $S(x, y)$ is point scatterers and $R = \{(x, y) : (x'_n - x)^2 + (y'_n - y)^2 = r\}$.

The image can be acquired by projecting out $E(r)$ in the (x,y) plane from each antenna position (x', y'), Figure 4.2.

$$I(x, y) \propto \sum_n P(E(R), x'_n, y'_n) \tag{4.2}$$

where $I(x, y)$ is a pixel in the image, P is a data point corresponding to antenna n and range R from the pixel.

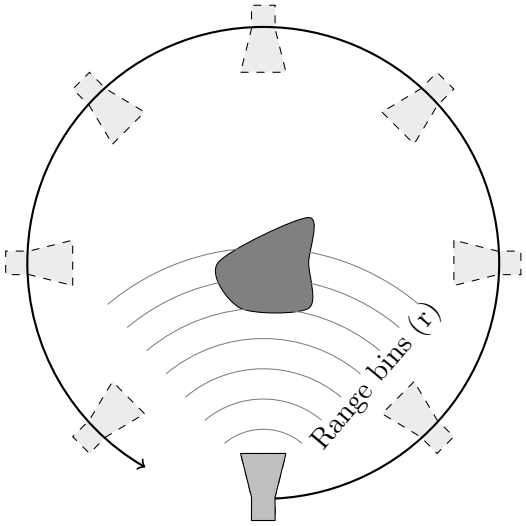

Figure 4.1: Eight antennas in a circle represent different antenna positions in a spotlight measurement. The curved lines show wavefronts from one of the antenna positions propagating into the scene of interest. The dark shape in the middle is the object to be measured.

The reason that backprojection works even though the data is collected for all points at a distance r is the synthetic aperture. In a point where there is a scatterer the signals are in phase for all antennas and the signals quickly becomes out of phase when moving away from a scatterer. This is the same principle as having a single antenna with high directivity that would only receive a signal from a small part of the object measured. A larger synthetic aperture will increase resolution until it reaches the limit set by the bandwidth of the signal.

The computational burden for backprojection is $k^2 \times L$, where for each pixel in the image $k \times k$, data from each antenna L must be added. The total complexity

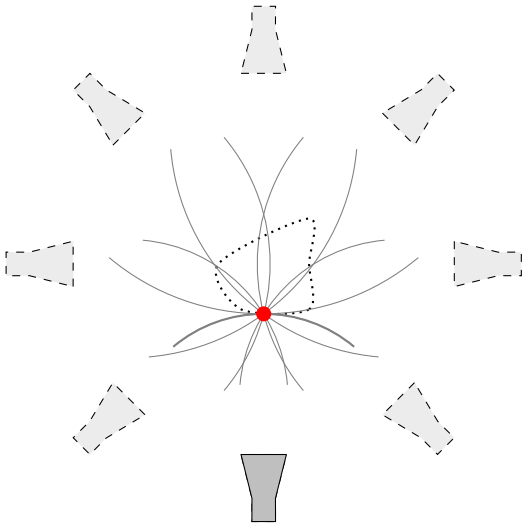

Figure 4.2: Illustration of the backprojection method in the spotlight case. The red dot is the current pixel for which a value is to be calculated. The gray lines are wavefronts from each antenna position (the highlighted thick line corresponds to the solid antenna in the bottom middle) where each line corresponds to one range bin in the data matrix. The value from each of these cells are added to the pixel.

is $O(n^3)$ [22]. The high complexity is the main disadvantage of the backprojection method and the algorithm is particularly slow for large data matrices. However, faster versions of the backprojection algorithm exist such as factorized backprojection [14].

4.1.2 Gridding

Gridding is a spotlight imaging algorithm that takes advantage of the Fourier transform [9]. Imagine that the object and antennas all are in a 2D plane (x,y). The image can then be seen as the 2D Fourier transform of $E(k_x, k_y)$. As the recorded time domain data is on the form $E(t, \theta)$, where t is fast time and θ is the measurement angle, the first step of the algorithm is to do a Fourier transform in fast time to obtain $E(f_r, \theta)$. This is then converted to the spatial frequency domain (k-space) by multiplying with a factor $2\pi/c$. The data is now on the form $E(k_r, \theta)$, where k_r is radial spatial frequency. To produce an image, which has down- and cross-range dimensions (x and y), the data first needs to be converted from polar coordinates (k_r, θ) to Cartesian coordinates (k_x, k_y). This is done by using the equations

$$k_x = k_r \cos(\theta) \tag{4.3}$$

$$k_y = k_r \sin(\theta) \tag{4.4}$$

where k_x and k_y are the Cartesian wave numbers, k_r is the radial wave number ($k_r = 2\pi f_r/c$), and θ is the measurement angle. The last step is to do a two dimensional Fourier transform to convert the data from the spatial frequency to the image domain.

The gridding method has a complexity $m \times L + k^2 + k^2 \log k^2$, where $m \times L$ is the size of the data matrix and k^2 is the number of pixels in the final image. $m \times L$ is required for polar to Cartesian conversion, k^2 for the interpolation and $k^2 \log k^2$ for the 2D FFT. The total complexity is $O(n^2 \log n^2)$ [23].

4.2 Implementations

In this section the imaging implementations for backprojection and gridding are explained, as well as methods to generate simulated data to test the methods.

4.2.1 Preprocessing

Initially all data is treated in the same way regardless of what imaging algorithm is to be used. First, SNR of the measured data is increased through matched filtering, where the filter is the recorded pulse shape from Figure 3.5 (where everything except the main pulse has been removed). Since the SNR is already high because of long measurement times, this step is not crucial. However, if one would do faster measurements the matched filtering could allow for a pulse shape to be detected and recreated from a signal that seems like pure noise, as long as the reference pulse has high enough SNR. The matched filtering is done by cross correlating the time domain signals from measured object and reference. Since the distance of the reference plate is known, this can be used to transform the fast time axis of the data matrix into distance. Data corresponding to distances beyond twice the object distance (multiple reflections as seen in Figure 3.5 (a)) is cropped to avoid unwanted clutter in the image. For a data matrix of size $m \times n$, the time per fast time index is

$$\Delta t = t_{max}/m = 10 \text{ ns}/8000 = 1.25 \text{ ps} \tag{4.5}$$

where t_{max} is the maximum time in the fast time vector (10 ns for all measurements) and m is the number of elements in the fast time vector (usually 8000). The distance per index is then (according to Equation 2.6

$$\Delta d = \Delta t \cdot c/2 = 0.1875 \text{ mm} \tag{4.6}$$

Figure 4.3 shows the data after filtering and cropping. Using the reference plate distance is only necessary to get an absolute distance on the scales of the final image, however relative distances within an image can always be calculated using Equation 4.6. In the case that the zero position is chosen to be centered around the object of interest, the absolute distance can be ignored.

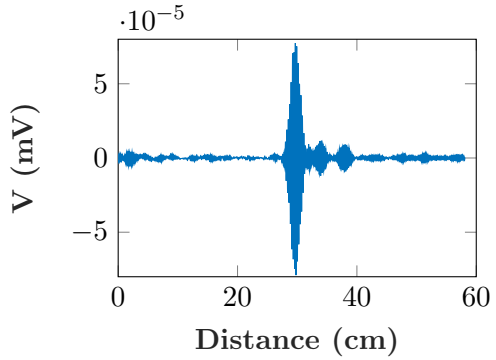

Figure 4.3: Filtered and cropped fast time data vector where the distance for each fast time index has been defined.

4.2.2 Backprojection

After the preprocessing the data is on the form of a $m \times n$ matrix, where m is the distance from different antenna positions n. m is ranging from zero to twice the object distance.

First an image matrix $I(x, y)$ is created with dimensions $k \times k$, where k represents the same spatial length as m. The coordinates for each antenna n is defined in the image grid, then for each pixel the distance to every antenna position is calculated and the corresponding data value at range m is added to that pixel, see Figure 4.2. It is beneficial that $k > m$ since this reduces the error from rounding the pixel distance to the nearest data range bin. The resulting image matrix is plotted as a two dimensional image where the color scale represents the value of each matrix cell. The dB scale is normalized to the maximum value in the matrix.

In the strip-map version of the backprojection method all the antenna positions are at a constant down-range while the cross-range changes for each position. The total path of a pulse is the sum of the distance from transmitter to the pixel plus the distance from pixel to receiver (Figure 4.4). Here the quasi-monostatic setup is taken into account, where the transmitter and receiver has a 5.5 mm spacing. For the spotlight version of the backprojection method the image formation process is similar to the strip-map case only that the coordinates for the antenna positions differ. In spotlight, all the antenna positions are at a constant radius while the angle changes for each position. This means that the antenna positions can be described by (r, θ). Here the quasi-monostatic setup is also taken into account. To focus the image the distance from the radar to the center of rotation (CoR), defined as d, needs to be manually defined in the script. This selects which down-range bin in the data matrix that is defined as the center.

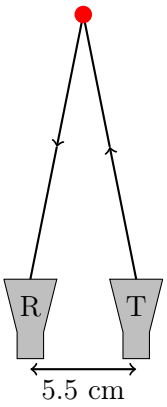

Figure 4.4: For a quasi-monostatic setup the path from transmitter to pixel and back to the receiver is the total distance, which corresponds to a single fast time index (according to Equation 4.5).

4.2.3 Gridding

The gridding method is implemented only for spotlight measurement data. After matched filtering, the data is Fourier transformed in fast time using an FFT. At this point the data is on the polar form $P(k_r, \theta)$, where k_r is radial spatial frequency and θ the measurement angle. The data has been collected over a set of angles, where the radius of each cell corresponds to the fast time. The data is then phase shifted by an amount corresponding to d, by multiplying each frequency bin by a factor e^{-ikd}, where k is the wavenumber for each bin. The reason this is done is that it is required for a point scatterer to be focused in the image. If it is not shifted the point would become a circle in the image since the mean value of the position in the data matrix is non-zero. The shift is very sensitive and the value has to be tweaked manually to find the correct focus. It is often not enough to measure the distance from radar to CoR in the setup. Note that the gridding method does not take the quasi-monostatic setup into account. However this effect decreases with higher d.

The next step is to convert the data from polar coordinates into Cartesian coordinates. In order to simplify this procedure when the data contains both positive and negative frequencies, the negative frequency components are first folded and added onto the corresponding frequencies in the positive half. This reduces the total dimensions of the data matrix and means that the Cartesian conversion can be done for a data set with frequencies from zero to f_{max}. The data in the spatial frequency domain and Cartesian coordinates (k_x, k_y) is shown in Figure 4.5 (a). As can be seen the data plotted in a Cartesian grid results in lines going radially outwards from the middle, where each line corresponds to a measurement angle. For each line only the radii corresponding to a certain frequency range (20-80 GHz) have non zero values. The reason is that in the algorithm, frequencies outside this range has manually been removed. This is because the cables have a

cutoff frequency of around 70 GHz (the data at these lower and higher frequencies is unwanted noise and not a part of the measured scattered signal from the object of interest). Using interpolation where each empty cell between the lines are filled based on the nearest values we get the interpolated data matrix in Figure 4.5 (b). The interpolation is done by convolving the data with a weighting function, which

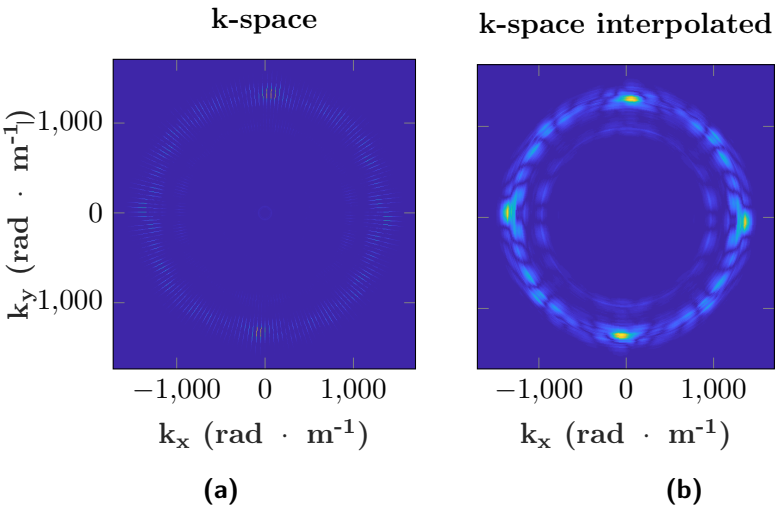

Figure 4.5: (a): Data matrix in spatial frequency domain (k-space) and Cartesian coordinates. (b): Interpolated k-space.

is a Kaiser-Bessel window, with α chosen according to Equation 2.16. This function, shown in Figure 4.6, weighs the data points closest to the current cell more than points further away.

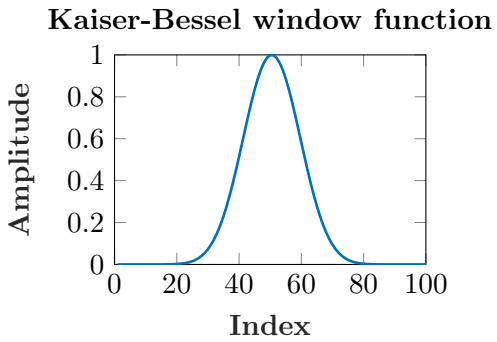

Figure 4.6: Weight function used to interpolate the data matrix after polar to Cartesian conversion.

After interpolation all the cells within a certain frequency range have values and the data is equidistant, which is a requirement for the FFT. The final step is to go from the spatial frequency domain (k_x, k_y) to the image domain (x,y). This

is done with a two dimensional Fourier transform (2D FFT), which results in an image matrix with complex data. In order to to visualize the complex data, the absolute values are displayed in a two-dimensional color map image similar to the backprojection images (also in dB scale).

Flowcharts summarizing the implemented backprojection and gridding methods are shown in Figure 4.7.

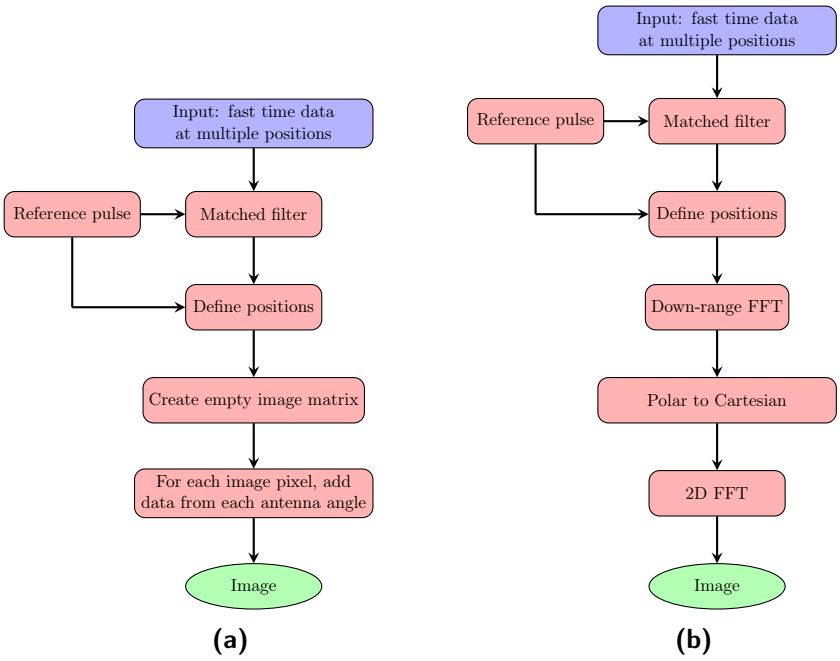

Figure 4.7: Flowcharts showing the major steps of the implemented imaging methods. (a) Backprojection. (b) Gridding.

4.3 Simulations

To be able to verify if the implemented algorithms work as intended scripts were made to simulate ISAR data for point scatterers in both strip-map and spotlight measurements. The simulated data should be ideal in the sense that one point scatterer corresponds to a single pixel regardless of what imaging method is used. If the algorithms are correct the point scatterer should therefore show up as a bright dot in the image.

In the simulation scripts the the transmitted pulse is a sine wave with one period where the pulse width can be chosen (for simplicity a Gaussian pulse can also be used to avoid negative values). A shorter pulse means that the dot from a point scatterer will be more focused in the image since the resolution is higher according to Equation 2.8 and 2.9.

4.3.1 Strip-map

For a strip map measurement a point scatterer is moving at the same down-range distance at all times, as shown in figure 2.5 (a). However, the cross-range position changes during the measurement as the object is moving sideways in front of the radar. The total range is therefore

$$R = \sqrt{x^2 + y^2} \tag{4.7}$$

where x is the cross-range position and y is the down-range position. Using Equation 2.6 R can be converted to fast time, which makes up the vertical axis of the data matrix (each row in the matrix is called a range bin). The further the radar is from the moving object, the less effect the change in x will have on the total range/fast time. The simulated data matrix for a moving point scatterer is shown in Figure 4.8 (a), where the down-range distance is 25 cm and the scan range is 18 cm. The apparent line is made up of many pulses (starting at slightly different fast times since the range changes for each x according to Equation 4.7). In this

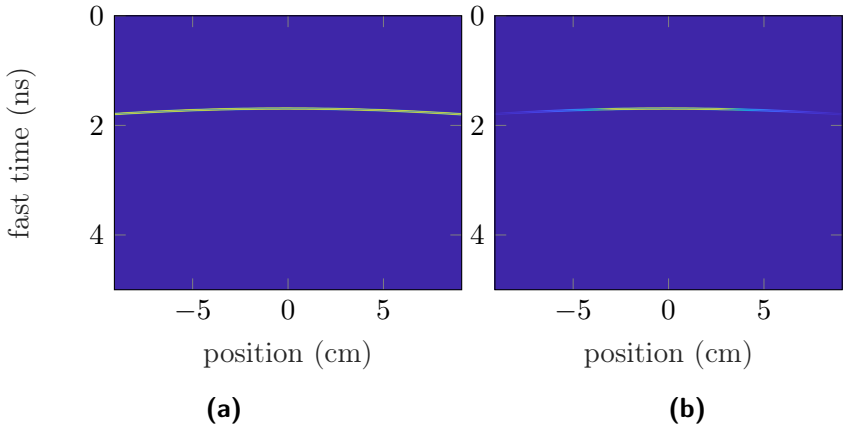

Figure 4.8: (a): Simulated data matrix for a point scatterer in a strip-map measurement. (b): When taking antenna gain vs angle into account.

example the signal amplitude of the scatterer at each cross-range is the same (the whole line has the same brightness) but in reality this is not the case considering that the antenna gain has an angular dependence. The result in Figure 4.8 can now be modified by multiplying the amplitude by the antenna gain in Figure 3.3 at 60 GHz (typical frequency used in a measurement), where the gain for each cross-range position x corresponds to the angle $\varphi_t = \arctan(x/y)$. This yields the simulated data in Figure 4.8 (b). Note that the attenuation due to higher range when further from the middle is not taken into account.

The strip-map backprojection method was tested using simulated strip-map data for multiple point scatterers placed with equal spacings at different cross-ranges. Figure 4.9 shows the resulting image using the simulated data. The scan range is 18 cm, divided into 90 steps and the down-range distance from radar to

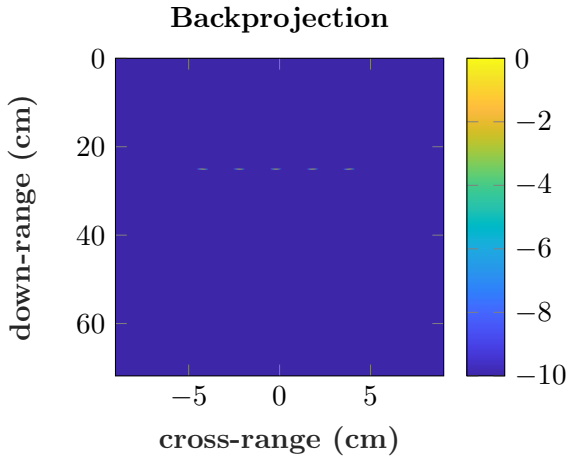

Figure 4.9: Image of five point scatterers using simulated data and the strip-map backprojection method. The scan range is 18 cm.

the scatterers is 25 cm (a setup similar to the real measurements). As can be seen in the image, each scatterer is correctly placed at the same down-range and at different cross-ranges. However, since the scan range is only 18 cm, the cross-range resolution is low (large Δx according to Equation 2.10). A higher resolution is obtained by having a larger scan range.

4.3.2 Spotlight

In a spotlight scan any point scatterer not in the center will be moving in a circle. Depending on where on the circle the point is the down-range distance from radar to the scatterer is different. Figure 4.10 shows two point scatterers in a rotating scene and the corresponding data matrix, where the fast time has been converted into range using Equation 2.6.

As can be seen in Figure 4.10 (b), the data for a scatterer moving in a circle in space corresponds to a sine wave in the data matrix. The y-coordinate of a scatterer corresponds to the amplitude, while the angle corresponds to the phase. However, this assumption is only true when the d is infinite (and the total range can be seen as being purely down-range). In reality, the total distance from radar to scatterer is described by

$$R = \sqrt{x^2 + (y + d)^2} \tag{4.8}$$

where x and y are the coordinates of the scatterer relative to the CoR. The larger the radius is and the smaller d is, the more effect x will have on the total range according to Equation 4.8. An example of the path of a scatterer in the data matrix when taking this effect into account is shown in Figure 4.11. In this example the scatterer is moving in a circle with the radius 1 cm and d is 2 cm. As can be seen, even with the radar positioned unrealistically close to the target compared to the radius at which the scatterer is moving, the effect is not very significant.

Still, the effect is included in the simulation algorithm in order to correctly test the imaging algorithms for scatterers at any radius and distance. The gain-angle dependence in Figure 3.3 has been disregarded since the object is assumed to be in the antenna main beam at all times during a spotlight scan.

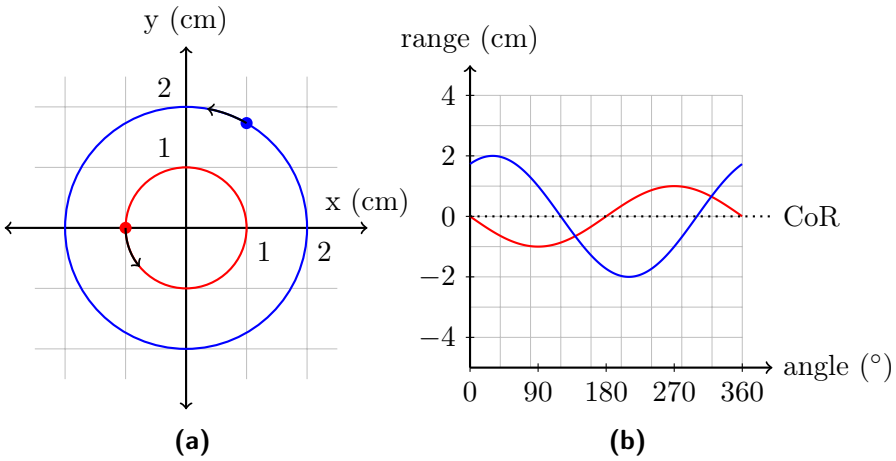

Figure 4.10: (a): A scene with two points scatters during a 360 degree spotlight measurement. The red and blue circles show the path of the scatters during the measurement. (b): Corresponding simulated data matrix for the two point scatterers. The vertical axis in the data has been converted from fast time to range using Equation 2.6. Note that in this illustration only the scatterer's y-component is contributing to the amplitude of the sine waves.

The spotlight backprojection method was tested using simulated spotlight data for multiple point scatters at different radii, see Figure 4.12 (a). As seen in the figure, all points are focused and have the same size and shape regardless of where they are in the image.

The gridding method was tested using the same simulated data as for the backprojection method. The resulting image using the gridding method is shown in Figure 4.12 (b). As can be seen the dots further from the middle gets distorted in the image. This problem comes from the fact that the cross-range position of each scatterer is not taken into account in the algorithm. As described in the simulations section, the path of each point scatterer in the data matrix is not a perfect sine wave. Using Fourier transforms (in which only a sine wave is transformed into a Dirac delta function which is infinitely narrow), the distorted sine waves of a moving scatter will therefore not become a focused dot in the image. The effect gets worse as the radius of the circle on which the scatterer is moving increases. It seems that at a radius above 10 cm the point scatterer splits in two. The dots close to center are not affected as much, since x is small compared to d (see 4.8). In order to avoid this the objects needs to be small and be at sufficient range from the radar. According to the simulated data in Figure 4.12 (b) this

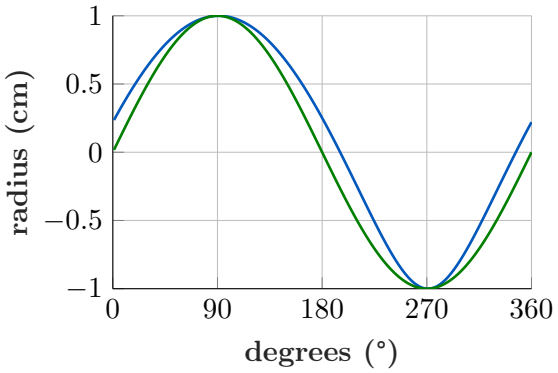

Figure 4.11: The blue curve shows a point scatterer in the data matrix when taking the scatterer's x coordinate into account. The green curve is the case when d is infinite and only y affects the total range (a perfect sine wave).

condition is approximately satisfied when the ratio between the distance to the object and object radius is above 7.5. Note that in the backprojection method this is not an issue, as seen in Figure 4.12. The reason is that the cross-range position of each moving scatterer is taken into account in the algorithm, similar to how the data was generated in the first place.

A way to solve the distortion problem could be to use another transform which takes the cross-range position into account. An example is the Fresnel diffraction equation, which is an approximation that can be applied to the propagation of waves in the near field.

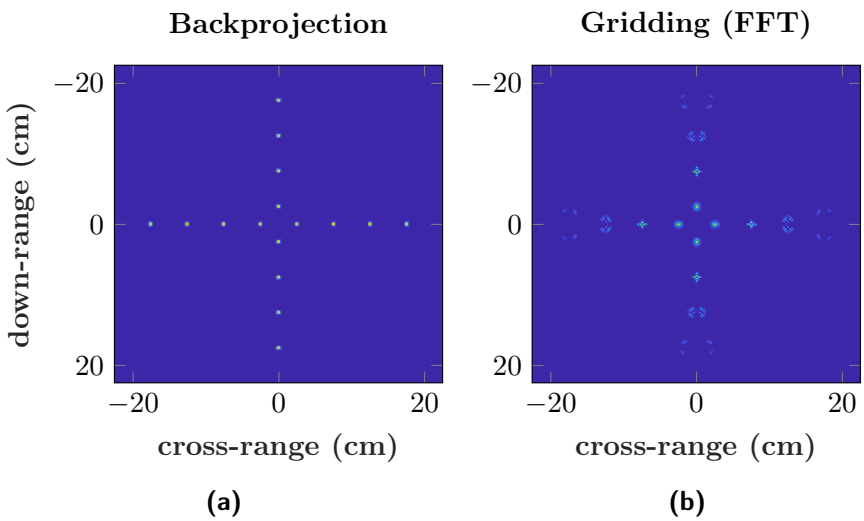

Figure 4.12: Image of point scatterers using simulated data for a spotlight measurement. d is 75 cm. a) Backprojection. b) Gridding. Points get more distorted the further from the middle they are.

Chapter 5
Results and Discussion

In this chapter, the resulting images using the implemented imaging methods on measurement data from a variety of objects are presented. The radar measurements, algorithms and results are also discussed.

5.1 Strip-map Images

Table 5.1 shows the parameters for the strip-map measurements.

Figure	Object	Distance (cm)	Scan details
5.1	3 cm metal strip in Fig. 3.7	25	91 steps, 18 cm
5.1	6 cm metal strip in Fig. 3.7	25	91 steps, 18 cm
5.3	metal profile in Fig. 3.8	25	91 steps, 18 cm
5.2	3 and 6 cm metal strips	32	200 steps, 20 cm

Table 5.1: Measured objects using a strip-map setup. All measurements were done using 5000 pulse averages.

Figure 5.1 (a) and (b) show strip-map backprojection images of two metal plates of widths 3 and 6 cm respectively. The widths in the images (cross-range) correctly show the physical widths. The down-range position of the object is also correct. However, in strip-map images there is no information (in down-range) about the thickness of an object. For example the thickness of a metal plate can not be retrieved from the data since there is no scattered field returning from the far side of the plate. The apparent thickness of the plates in figure 5.1 is a result of the pulse width not being infinitely short. This is in comparison to the image of simulated data in Figure 4.9, where the pulse is only one period and much shorter, which results in the scatterers being more focused in down-range.

Figure 5.2 shows an image of both the 3 and 6 cm strips, separated by 2 cm in down-range and 2.5 cm in cross-range. The objects are clearly distinguishable and both the widths and separation are correct. Even if the left metal strip is half as wide, its amplitude is higher, which is counterintuitive since it should reflect less than the wider plate. One explanation for this might be that the 3 cm wide metal plate is in the resonance region for scattering. In figure 2.2, this would correspond to one of the maxima in the resonance region.

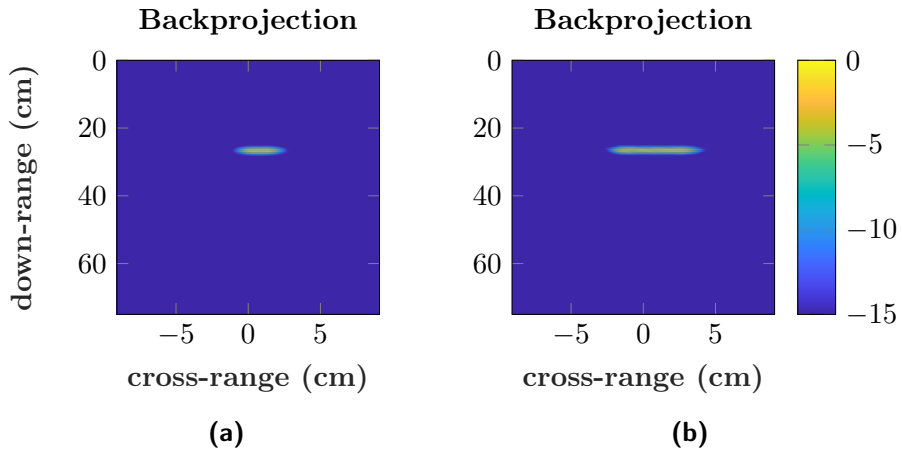

Figure 5.1: Images of metal strips using strip-map measurement data and backprojection algorithm. Colorbar in dB and normalized to max value. (a): 3 cm width, (b): 6 cm width

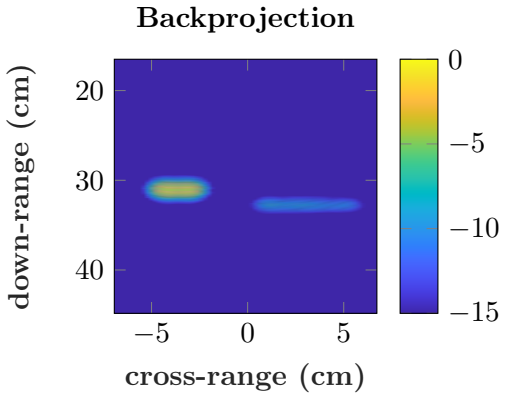

Figure 5.2: Image of two metal strips (3 and 6 cm width) using strip-map measurement data and backprojection algorithm. The colorbar is in dB scale and normalized to max value.

In Figure 5.3 an image of the metal profile in Figure 3.8 is shown using a strip-map measurement and backprojection method. The flat side of the profile is away from the radar, meaning that the side facing the radar has a groove in the middle. While the width of the profile is correct, there are no visible features of the groove. The reason for this might be that the cross-range resolution is too low for a strip-map measurement. From table 5.1, the scan angle can be calculated to $\arctan(9/25) \cdot 2 = 40$ degrees but as seen in figure 3.3, the 3 dB beam width at 60 GHz is approximately 20 degrees and will limit the observation angle Φ. Using Equation 2.10 with an observation angle Φ of 20 degrees and a λ of 5 mm, the cross-range resolution Δx is calculated to 7.3 mm. The calculated resolution is

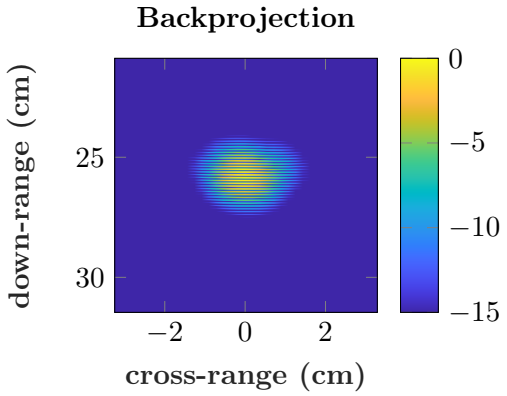

Figure 5.3: Image of the metal profile in Figure 3.8 using strip-map measurement data and backprojection algorithm. The colorbar is in dB scale and normalized to max value.

on the same order of magnitude as the groove width in the profile and this might explain why we can not distinguish it. A longer scan-range might have lead to a higher resolution and a visible groove. Compared to a spotlight measurement, we do not get any information about the far side or sides of the object in a strip-map measurement. Note that the thickness (in down-range) in the image is due to the length of the radar pulse and not the physical depth of the object. In this case it is merely a coincidence that the apparent thickness is the same as the physical depth. The horizontal dark lines in the object in Figure 5.3 is a result of the zeros of the measured pulses which are present after the signals are summed.

5.2 Spotlight Images

Table 5.2 shows the parameters for the spotlight measurements.

Figure	Object	Distance (cm)	Scan details
5.4	metal profile in Fig. 3.8	30	180 steps
5.5	metal profile and PMMA-rod in Fig. 3.9	35	180 steps

Table 5.2: Measured objects using a spotlight setup. All measurements were 360° scans using 5000 pulse averages.

Figure 5.4 shows images of the metal profile in Figure 3.8 using spotlight measurements, where (a) is using the backprojection method and (b) is using the gridding method. Comparing Figure 5.4 (a) and Figure 5.3, a large difference can be seen in image quality between strip-map and spotlight backprojection images. In figure 5.4 (a) sharp corners can be seen and the grooves are also distinguishable while figure 5.3 only shows a bright area with no features but correct width. For

spotlight mode, the down-range resolution is equal to the cross-range resolution as discussed in the Section (2.4.2). According to Equation 2.8 and 2.9, the down-range resolution with pulse width 80 ps is 6 mm. The large difference in image quality between strip-map and spotlight seems to not correspond to the calculated values if the cross-range resolutions are considered, 7.3 mm for strip-map and 6 mm for spotlight. Theoretical calculations of resolution, both for cross- and down-range, are always an estimate since the bandwidth definition is arbitrary and the frequencies in a pulse are spread over a large range.

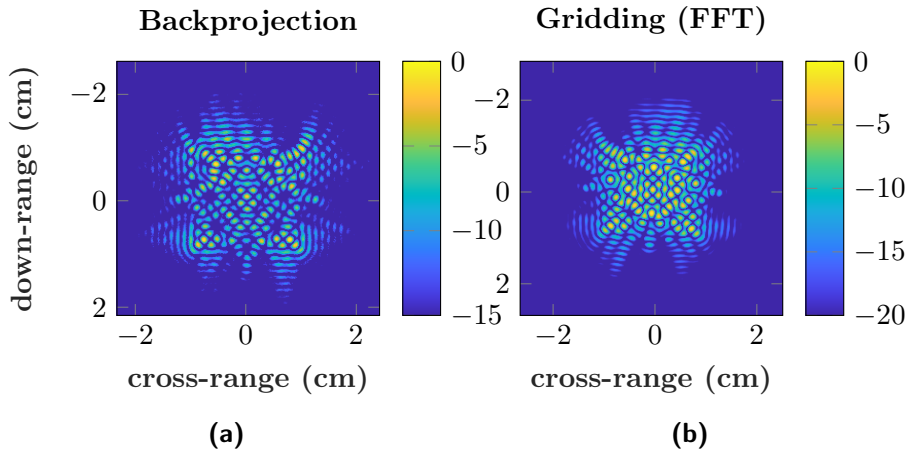

Figure 5.4: Image of the metal profile in Figure 3.8 using spotlight measurement data. The colorbar is in dB scale and normalized to max value. Backprojection method (a). Gridding method (b).

Comparing the two spotlight images in Figure 5.4, more details can be seen in the backprojection image. Especially the corners are more visible than in the gridding image. The reason might be a focusing issue when defining the CoR in the gridding image, but it might also be a result of the distortion from Figure 4.12 (b). However, since the object is at 30 cm distance and the radius of the object is approximately 1.4 cm, the ratio of distance-to-object radius is 30/1.4 = 21 which is higher than the limit 7.5, as determined from the simulated data image in Figure 4.12 (b). Therefore the metal profile is small enough compared to its distance from the radar to not be distorted. Another reason for the lower image quality might be that the frequencies outside the range 20 to 80 GHz were removed in the gridding algorithm.

The same radar and object were also used in radar measurements done by Iman Vakili [15]. In his work, measurements were done in both time domain, using a sampling oscilloscope and in frequency domain using a vector network analyzer (VNA). The images based on time domain measurements and the gridding method looks similar. However, further techniques to boost the quality were used such as zero force equalization, where the side lobes of the Fourier transformed signal are boosted by dividing the signal by the power spectral density of the time-domain

reference signal. This resulted in a higher resolution image where more detailed features can be seen. It is also mentioned that zero-forcing suffers from noise enhancements and use of this method has to be avoided when the SNR is low. When comparing to our backprojection image, the corners in the backprojection image are sharper and more defined than in Iman's image. In backprojection, the edges of the outer structure are straight line whereas the edges are rougher in Iman's image. The VNA measurements resulted in high resolution images, with $\Delta x = \Delta y = 3$ mm due to the wide bandwidth of the VNA with approximately constant power level at all frequencies. Judging from his image, the use of a VNA seems to have provided an image that more accurately represent the shape of the object.

Figure 5.5 shows images of the metal profile (4 cm from the center) and an acrylic glass (PMMA) rod (2.8 cm from the center), both being attached on a rotating plate. In the backprojection image in Figure 5.5 (a) the metal profile visible in the upper right corner. However, the PMMA rod in the lower left is barely visible. It looks like a large circle, while also being smeared out. The reason is that compared to metal, PMMA is not conductive and is semi transparent to millimeter waves. The ghost features in the image are likely due to data from multiple reflections inside the PMMA rod, at the front and back. The backprojection algorithm is based on only direct paths to and from a scatterer, which is why the multiple reflections show up as curved lines in the background. As can be seen in Figure 5.5 (b), the resulting image using the gridding method is not as resolved as the backprojection image. Also the PMMA rod is barely visible. A reason for this might be the distortion related to larger object scenes. Since the rotating scene with the two objects have a total radius of 5 cm, the distance-radius ratio is $35/5 = 7$, which is slightly below the determined limit for distortion. Therefore, the data from this particular measurement is not suitable for using the gridding method.

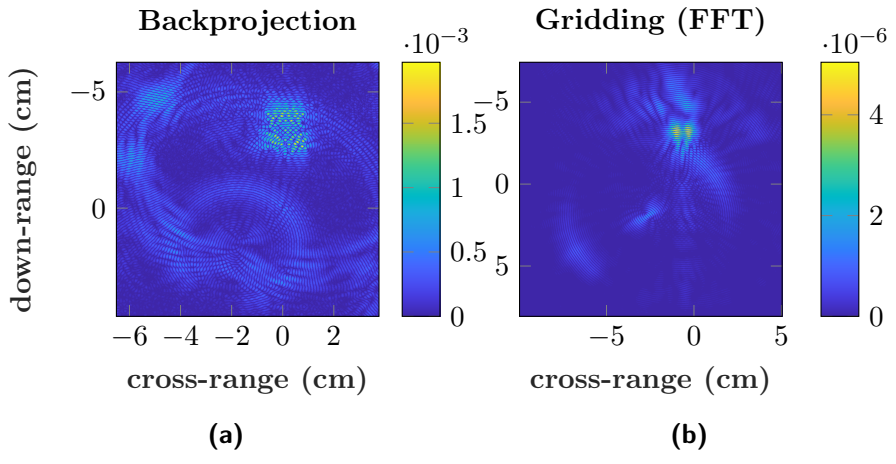

Figure 5.5: Images of the metal profile and PMMA rod in Figure 3.9 (b) using spotlight measurement data. The colorbar is in linear scale. (a) Backprojection method. (b) Gridding method.

An important difference between the backprojection and gridding algorithms is their computational complexity. The backprojection was estimated to have a complexity of $k^2 \times L$ while the gridding method had a complexity of $k^2 \log(k^2)$. From this gridding seems to be faster since $\log(k^2)$ is most likely less than L. However, since gridding is a frequency domain method all data (in a certain frequency range) in the frequency domain must be used to create the image in order to not lose resolution. The backprojection on the other hand does not have this requirement, therefore only a limited part of the image can be constructed. This can make the backprojection faster in some cases if the radius of the limited image is small enough. In Figure 5.4 $L = 180$ and $k = 3200$ for both (a) and (b). For this case it is true that $\log(k^2) < L$. However, in (a) the radius was limited to 3.5 cm, which corresponds to $3.5/\Delta d = 187$ indices. The total complexity for (a) is now $\pi k_r^2 L = 2 \cdot 10^7$, where πk_r^2 is the number of pixels contained within the circle with radius k_r. The total complexity for gridding is $k^2 \log(k^2)$ is $7 \cdot 10^7$. This means that the backprojection method is faster in this case. If we would not limit the radius, the backprojection would have a total complexity of $184 \cdot 10^7$ and gridding would be faster.

5.3 Uneven Sampling and Interpolation

Another limitation of the FFT is that it requires equidistant samples. If a signal equal to a wave function $f(x)$ has been sampled irregularly to a discrete function $s(x)$, Figure 5.6 (a), and an FFT is to be performed, simply using the sample points will cause the FFT to assume that it is fed the function $g(x)$, Figure 5.6 (b), which does not represent $f(x)$. If zeros are placed at an interval equal to the shortest sampling distance where sample points are missing, the problem is partially solved. The samples are now evenly spaced and taking the integral $\int s(x)f(x)dx$ will result in a large amplitude. Ideally the previous integral should be zero if $f(x)$ is replaced by an orthogonal wave function but since there are more samples left of the first node, other wave function will also result in an amplitude other than zero. This will lead to a broadening of the peak in the frequency domain. Replacing the zeros with an estimate of $f(x)$ or sampling more often will reduce this effect. In our setup no difference was seen between interpolated and non interpolated images, Figure 5.7 (a) and (b). With 180 angles sampled, we probably have enough samples so that the broadening of the peaks does not limit our resolution.

If fewer angles were used the images started to lose resolution. This can be seen in Figure 5.7 (c) where only 60 angles are used. With few angles interpolation started to make a difference. In Figure 5.7 (d), the 60 angles has been interpolated to 180 using Matlab's resample algorithm and the image quality is greatly improved. In Figure 5.7 (e) our own interpolation algorithm was used to increase the angles from 60 to 180. In this method the angles were convoluted with a Kaiser-Bessel window. This gave a better image than before interpolation but a worse image than when using Matlab's resample. The implemented interpolation method for the gridding method focused on optimizing speed. In this method the algorithm goes through each pixel in the empty k-space and calculates the angle and radius for the pixel. The sampled data points closest to this polar coordi-

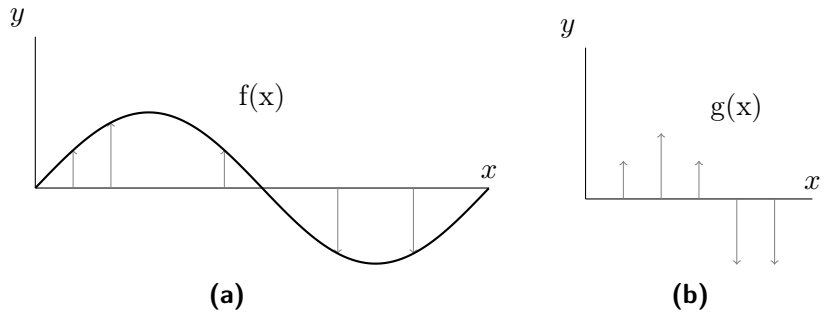

Figure 5.6: (a): $f(x)$ is a continuous sinusoid and the vertical lines are non-equidistant samples of $f(x)$. (b): How the FFT will interpret the samples take in (a), note that this no longer represents $f(x)$.

nate are then weighted and added to the pixel. Using Matlab's resample, a lot of unnecessary data would be created, especially for short radii. This would add extra time to the algorithm since not all new created data points would be used to fill the k-space. However, it could also be that our interpolation algorithm is not completely correct and needs some improvement.

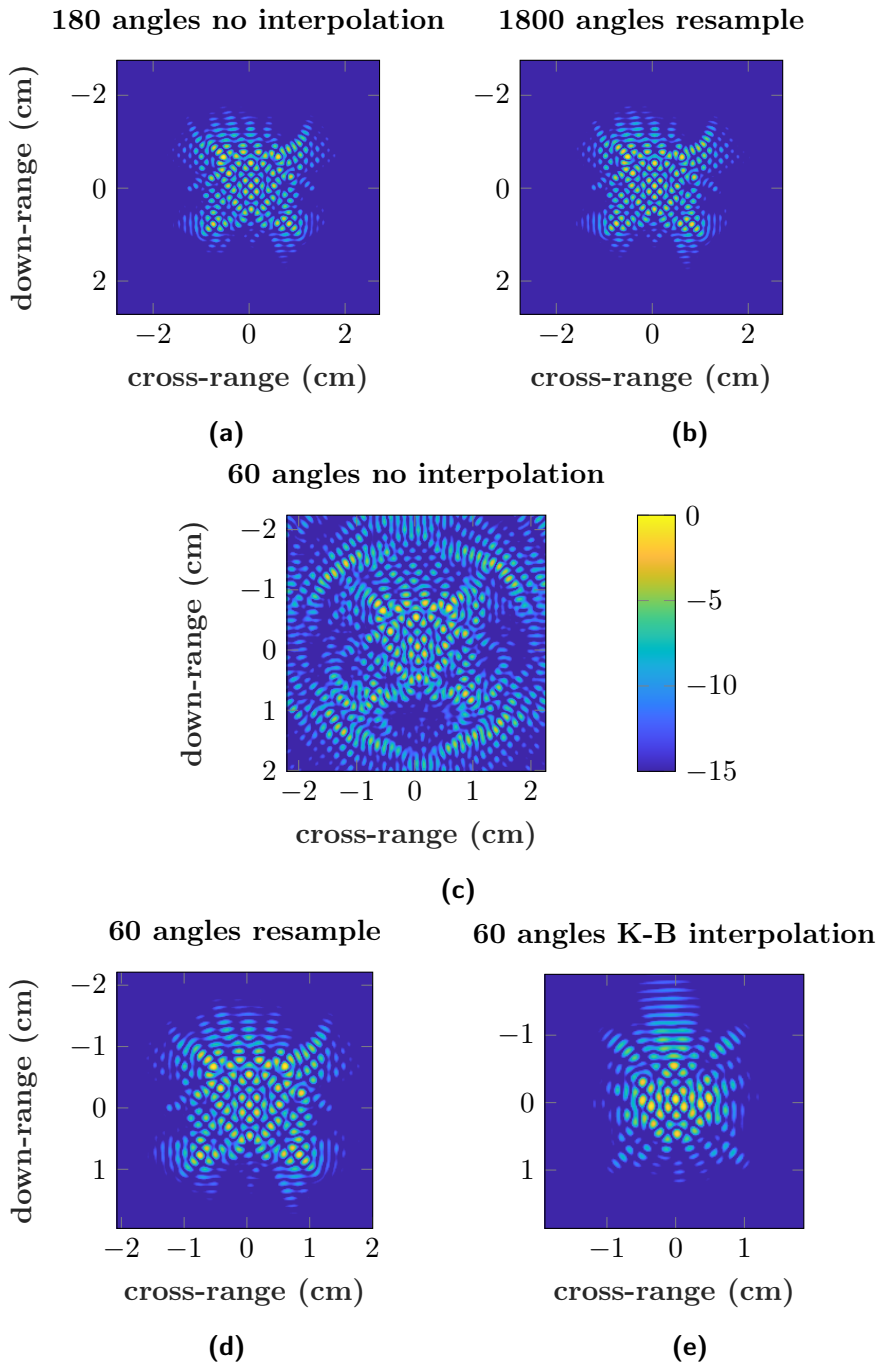

Figure 5.7: Images of the metal profile seen in Figure 3.8 using spotlight measurement data and the gridding method. (a) using the original 180 angles and no interpolation. (b) the original data is interpolated to 1800 angles using Matlab's resample. (c) only using 60 equally spaced angles and no interpolation. (d) using 60 equally spaced angles interpolated to 180 angles with Matlab's resample. (e) using 60 equally spaced angles interpolated to 180 angles with our own implemented method.

Chapter 6
Conclusion and Outlook

In this thesis we have done radar measurements using the two ISAR modes strip-map and spotlight. We have also implemented two different imaging algorithms, backprojection and gridding. The imaging methods were verified with simulated data and then used with radar measurement signal data in time domain. Strip-map resulted in images with no information about the object thickness and the cross-range resolution was low. However individual objects could be resolved a few centimeters from each other and each object width and down-range position were correct. Spotlight images resulted in higher resolution images with full 360 degree information of the object scene. Both backprojection and gridding algorithms are able to produce similar quality images with a resolution of less than one centimeter when used in spotlight mode. From its higher complexity, backprojection is slower than gridding when used to generate large images. On the other hand, the backprojection method can be faster if the object size is known and only a limited radius of the image needs to be shown. The gridding method has a lower complexity but can be used to generate images of similar resolution to backprojection. The main disadvantage with gridding is that objects with a small distance-to-radius ratio are distorted, which limits the object size for a specific distance.

The strip-map mode might seem inferior to the spotlight mode because of its lower resolution and observation angle. However, in a ISAR imaging application such as scanning human tissue in vivo for cancer cells, it would be easier to move a body part in a straight line in front of the radar instead of having to rotate the whole body, hence there is practical advantage of using the strip-map mode. Doing this in spotlight mode the setup would likely have to be SAR instead of ISAR.

Following the work in this thesis, a possible next step could be measurements being done using a bistatic setup, in which the transmitting and receiving antennas are placed at an angle to a surface. This technique is an advantageous way to analyze features on a surface since additional information about height can be obtained. This kind of topography measurement would require new bistatic imaging algorithms to implemented, either for strip-map or spotlight.

The measurements were done with a long integration time in order to get data with as high SNR as possible. High quality images could probably be obtained using lower integration time in order to make the measurements faster.

A problem during spotlight measurements was that it was hard to determine

the exact center of rotation from the setup, which affects both the backprojection and gridding algorithms. The reason is that the exact phase center within the leaky lens antenna is unknown. This means that even if the correct distance from the front of the antenna to the rotating actuator's center was measured, the value would still have to tweaked and iterated in the script in order to focus the image. Some procedure to optimize this such as an auto focusing Matlab script would have been beneficial.

One potential way to increase the resolution for any imaging method is a technique called zero-forcing equalization, where the amplitude of the side lobes of a signal are increased in amplitude. Doing this increases artifacts and noise but this is not a problem if the SNR is already high from having high integration time. Another way to improve resolution would be to use chirped pulses, in which the carrier frequency is swept during each pulse transmission. This is a way to increase the signal bandwidth and thus increase resolution according to Equation 2.8. However, with the transmitter circuit used in this thesis this is not possible. The frequency can be changed plus minus a few percent with the bias voltage, but not fast enough to be done during each pulse transmission.

By using a system where the transmitter, receiver and antennas are integrated, cables can be avoided which reduces noise, increases SNR and allows for high frequencies to be used. This would also be a requirement for a commercial applications in which the reduced size of the radar would allow it to for example be integrated in a mobile device. Less noise would also allow for fewer averages to be taken, which would result in faster measurements.

References

[1] S. J. Orfanidis, "Electromagnetic waves and antennas", Ch. 5 "Reflection and transmission", 2016.

[2] Waves and Frequency Ranges, http://www.radartutorial.eu/07.waves/Waves%20and%20Frequency%20Ranges.en.html Retrieved 2018-05-03.

[3] S. Heunisch, L. Ohlsson and L. E. Wernersson, "Reflection of Coherent Millimeter-Wave Wavelets on Dispersive Materials: A Study on Porcine Skin," in IEEE Transactions on Microwave Theory and Techniques, vol. 66, no. 4, pp. 2047-2054, April 2018.

[4] Intrapulse Modulation and Pulse Compression, http://www.radartutorial.eu/08.transmitters/Intrapulse%20Modulation.en.html Retrieved 2018-06-13.

[5] A. V. Oppenheim, R. W. Schafer "Discrete-Time Signal Processing" (3rd ed.), Pearson, 2014.

[6] Radar principle, http://www.radartutorial.eu/01.basics/Radar%20Principle.en.html Retrieved 2018-05-03.

[7] W. L. Melvin, J. A. Sheer, "Principles of modern radar Vol. II: Advanced techniques", SciTech Publishing, 2013.

[8] S. Heunisch, L. Ohlsson and L. E. Wernersson, "Reflection of Coherent Millimeter-Wave Wavelets on Dispersive Materials: A Study on Porcine Skin," in IEEE Transactions on Microwave Theory and Techniques, vol. 66, no. 4, pp. 2047-2054, April 2018.

[9] F. Andersson, R. Moses and F. Natterer, "Fast Fourier Methods for Synthetic Aperture Radar Imaging," in IEEE Transactions on Aerospace and Electronic Systems, vol. 48, no. 1, pp. 215-229, Jan. 2012.

[10] M. Egard, M. Arlelid, L. Ohlsson, B. M. Borg, E. Lind and L. E. Wernersson, "$In_{0.53}Ga_{0.47}As$ RTD–MOSFET Millimeter-Wave Wavelet Generator," in IEEE Electron Device Letters, vol. 33, no. 7, pp. 970-972, July 2012.

[11] Ross KF, Gordon RE., "Water in malignant tissue, measured by cell refractometry and nuclear magnetic resonance." https://www.ncbi.nlm.nih.gov/pubmed/7143438, 1982.

[12] C, Özdemir, "Inverse synthetic aperture radar imaging with matlab algorithms", John Wiley & Sons, 2012.

[13] M. O. Kolawole, "Radar Systems, Peak Detection and Tracking", Biddles, 2002.

[14] L. M. H. Ulander, H. Hellsten and G. Stenstrom, "Synthetic-aperture radar processing using fast factorized back-projection," in IEEE Transactions on Aerospace and Electronic Systems, vol. 39, no. 3, pp. 760-776, July 2003.

[15] I. Vakili, "Time-Domain Antenna and Scattering Analysis for Micro- and Millimeter-Wave", Lund University, 2015.

[16] C. A. Balanis, "Antenna Theory: Analysis and Design" (3rd ed.), Wiley, 2005.

[17] Armin W. Doerry, Edward E. Bishop, John A. Miller "Basics of Backprojection Algorithm for Processing Synthetic Aperture Radar Images", Sandia National Laboratories, 2016.

[18] M. A. Richards, J. A. Scheer, W. A. Holm "Principles of Modern Radar Basic Principles", SciTech Publishing, 2015.

[19] W. L. Melvin, J. A. Scheer "Principles of Modern Radar Vol. II: Advanced Techniques", SciTech Publishing, 2013.

[20] https://www.cv.nrao.edu/course/astr534/LarmorRad.html, 2008, Retrieved 2018-05-14.

[21] T. Courvoisier, "High Energy Astrophysics", Springer, 2013

[22] Y. F. Shao et al., "Fast Backprojection Algorithm for Bistatic SAR Imaging," in IEEE Geoscience and Remote Sensing Letters, vol. 10, no. 5, pp. 1080-1084, Sept. 2013.

[23] L. Feng et al., "The Gridding Method for Image Reconstruction of Nonuniform Aperture Synthesis Radiometers," in IEEE Geoscience and Remote Sensing Letters, vol. 12, no. 2, pp. 274-278, Feb. 2015.

[24] https://www.ias.ac.in/article/fulltext/reso/004/02/0020-0023, 1999, Retrieved 2018-05-24.

[25] https://www.cv.nrao.edu/course/astr534/AntennaTheory.html, Retrieved 2018-05-26.

[26] P. J. Beatty, D. G. Nishimura and J. M. Pauly, "Rapid gridding reconstruction with a minimal oversampling ratio," in IEEE Transactions on Medical Imaging, vol. 24, no. 6, pp. 799-808, June 2005.

[27] http://www.radartutorial.eu/01.basics/Rayleigh-%20versus%20Mie-Scattering.en.html , Publisher Christian Wolff, Retrieved 2018-05-31.

Appendix A
Matlab code

A.1 Simulated data

A.1.1 Figure 4.8 (a) and (b)

```
%One point scatterer
%18 cm scan distance
data=simullindatascatterer(8000,90,2,40);
x=linspace(-9,9,90); %scan distance from -9 to 9 cm
y=linspace(0,8000*1.25e-3,8000); %convert time index
    to time in ns

imagesc(x, y(1:4000), abs(data(1:4000,:)));
xlabel('position (cm)');
ylabel('fast time (ns)');

function [data] = simullindatascatterer(a,b,
   pulsetype,pulselength)

data=zeros(a,b);

deltaT=10e-9/size(data,1);
deltaD=deltaT*3e8/2;

%Pulse shape
if pulsetype==1
    g=gausswin(pulselength);
end
if pulsetype==2
    gx=linspace(0,2*pi,pulselength);
    g=sin(gx)';
end
```

```
%Points
dXscan=0.18/b; %scan steps
y=0.25; %down-range distance to scan line

for j = 1:b
    x1=0.1175-j*dXscan; %x-dis transmitter
    x2=0.0625-j*dXscan; %x-dis range receiver

    d1=sqrt(x1^2+y^2); %dis transmitter
    d2=sqrt(x2^2+y^2); %dis receiver

    d=round((d1+d2)/2/deltaD); %total distance (
        halved)

    anglet=abs(rad2deg(atan2(y,x1))-90); %angle to
        transmitter
    angler=abs(rad2deg(atan2(y,x2))-90); %angle to
        receiver
    gaint=0.9985*exp(-0.1158*anglet); %gain
        transmitter
    gainr=0.9985*exp(-0.1158*angler); %gain receiver
    gain=gaint*gainr; %total gain to object and back

    data(d:d+pulselength-1,j)=data(d:d+pulselength-1,
        j)+g; %add point data to data matrix
%    data(d:d+pulselength-1,j)=data(d:d+pulselength
    -1,j)+g*gain; %add point data to data matrix,
    with gain vs angle factor
end

end
```

A.1.2 Figure 4.11

```
points=[60 180];
r=1;
CoR=2;
for k=1:360
    ang=deg2rad((k-1)+180);
    ty=CoR-r*sin(ang);
    tx=r*cos(ang);
```

```
    t(k)=(sqrt(ty^2+tx^2));
end
t2=r*sin(deg2rad(1:360));
t=t-CoR;
x=linspace(0,4.5,360);
hold on;
plot(t);
plot(t2);
grid on;
s = sprintf('%c', char(176));
xlabel(['degrees (' s ')']);
```

A.2 Matched filtering

The following code is used in the beginning of each imaging algorithm to filter the data and set a reference distance.

```
%Load reference and object measurement data
%Here they are referred to as 'ref' and 'data'
%Both are matrices with rows being fast time,
%cols being position/angle
%and each cell value is the measured voltage
%t is a vector with the time for each fast time
    index
%'CoR' = center of rotation, is set manually (only
    for spotlight measurements)
%'refD' = reference plate distance, is set manually

deltaTime=t(2)-t(1); %time per fast time index (s)
deltaDist=deltaTime*3e8/2; %distance per fast time
    index (m)
totaltime=deltaTime*length(t); %total fast time span
     in data (s)

Tsampl=totaltime/size(data,1); %sampling time (s)
fmax=1/Tsampl/2*1e-9; % sampling frequency (GHz)

%Create matched filter from reference
[max_num, max_idx]=max(ref(:));
[X,Y]=ind2sub(size(ref),max_idx); %Find pulse
    position
ref(1:X-100)=0; %Remove parts outside pulse
ref(X+100:end)=0;
```

```
%Apply matched filter
filtered=zeros(size(data,1)*2-1,size(data,2));
for j=1:size(data,2)
    [filtered(:,j),lags]=xcorr((data(:,j)),(ref)); %
       lags is shift from convolution
end

half=size(data,1)/2;
filtered(find(lags==half):end,:)=[]; %remove half of
    convolution
filtered(1:find(lags==-half),:)=[];
lags(find(lags==half):end)=[];
lags(1:find(lags==-half))=[];

%Cut data to set downrange zero at antenna
range=lags*deltaD+refD; %affects antenna position a
   thus point trace in data
[~,j]=min(abs(range));
filtered(1:j-1,:)=[];
range(1:j-1)=[];
[~,j]=min(abs(range-2*CoR)); %remove double
   reflections
filtered(j:end,:)=[];
range(j:end)=[];
```

A.3 Strip-map

A.3.1 Figure 5.1 (a) and (b), 5.3 and 5.2

```
%Backprojection
F = filtered;

maxCR = scanDis;
deltaCR = maxCR/100;
CRscale = -maxCR/2:deltaCR:maxCR/2;

I=zeros(size(F,1),length(CRscale));

for Irad=1:floor(size(F,1)/2)
    Y=Irad*deltaD;
```

```
                                                %pixel Y
        -coordinate
    for Icol=1:length(CRscale)
        for antennaPos=1:s(2)
            X=(Icol-1)*deltaCR-maxCR/2;
                                %pixel X-coordinate,
               0 in middle

            Xa=(antennaPos-1)*scanStep-scanDis/2;
                     %antenna X position

            Xt=(Xa-0.0275)-X;
                                             %dX
               transmitter and pixel
            Rt=sqrt(Y^2+Xt^2);
                                            %dR
               transmitter and pixel

            Xr=(Xa+0.0275)-X;
                                             %dX
               receiver and pixel
            Rr=sqrt(Y^2+Xr^2);
                                            %dR receiver
                and pixel

            Rtot=Rt+Rr; %distance from antenna to
               pixel (Irad,Icol) and back

            Rindex=round(Rtot/deltaD/2);

            I(Irad,Icol)=I(Irad,Icol)+F(Rindex,
               antennaPos);
        end
    end
end

DRscale=range(1:size(I,1));

Idb=fliplr(db(abs(I))); %absolute value in decibels

maximg=max(max(Idb));
imagest(CRscale*100, DRscale*100, Idb-maximg, '
```

```
   Backprojection', 'cross-range (cm)', 'down-range
   (cm)');
caxis([-15 0]);
```

A.4 Spotlight

A.4.1 Figure 5.4 (a) and 5.5 (a)

```
%Backprojection
F=filtered;
I=zeros(size(F,1),size(F,1)); %image matrix

CoR=[size(F,1)/2 size(F,1)/2]; %center of rotation
antennaTrans=[0 size(F,1)/2-2.75/(100*deltaD)];
   %transmitter position
antennaRec=[0 size(F,1)/2+2.75/(100*deltaD)];
   %receiver position

maxIndexRadius=round(ImageRadius/deltaD);

for Irad=1:size(F,1)
    for Icol=1:size(F,1)
        r=sqrt((CoR(1)-Irad)^2+(CoR(2)-Icol)^2);
        if r<maxIndexRadius %limit radius of final
           image
            pixelAngle=atan2(Irad-CoR(1),Icol-CoR(2)
               )+pi/2-0.04;
            for antennaAngle=1:size(F,2)
                dcol=(antennaAngle-1)*360/size(F,2);

                ydis=CoR(1)-r*cos(pi*dcol/180+
                   pixelAngle)-antennaTrans(1)/2-
                   antennaRec(1)/2;
                xdis=CoR(2)-r*sin(pi*dcol/180+
                   pixelAngle)-antennaTrans(2)/2-
                   antennaRec(2)/2;
                drad=sqrt(xdis^2+ydis^2);
                  value=F(round(drad),antennaAngle);
                  I(Irad,Icol)=I(Irad,Icol)+value;
            end
        end
    end
```

```
end

dX=2*refD/size(I,1);
XYscale=-size(I,1)/2*dX:dX:size(I,1)*dX/2-dX;
XYscale=XYscale*100; %in cm

imgmax=max(max(db(abs(I))));
imagest(XYscale,XYscale,(db(abs(I))-imgmax),'
   Backprojection','cross-range (cm)','down-range (
   cm)');
caxis([-15 0]);
```

A.4.2 Figure 5.4 (b) and 5.5 (b)

```
%Fast time FFT
dataFFT=fft(filtered); %fast time FFT

s = [size(dataFFT,1), size(dataFFT,2)]; %phase shift
    coefficient
f=linspace(0,fmax,s(1)/2); %frequency vector 0 to
   fmax in Ghz
k=2*pi*f/0.3; %k vector
for i=1:s(2)
   dataFFT(1:s(1)/2,i)=dataFFT(1:s(1)/2,i).*exp(-2*
      pi*1i*k*CoR)'; %phase shift pos freqs
end
for i=1:s(2)
   dataFFT(s(1)/2+1:end,i)=dataFFT(s(1)/2+1:end,i).*
      exp(-2*pi*1i*k*CoR)'; %phase shift neg freqs
end

Wpos=dataFFT(1:end/2,:);

Wneg=flipud(dataFFT(end/2+1:end,:)); %flip neg freqs
Wneg=[Wneg(:,end/2+1:end), Wneg(:,1:end/2)]; %shift
   neg freq indices 180 degrees
dataShifted=Wpos+Wneg; %superpose pos/neg freq
   vectors

%Limit frequency range

fminInd=round(20/400*length(dataShifted));
```

```
fmaxInd=round(80/400*length(dataShifted));

han=zeros(size(dataShifted));
for j=1:s(2)
    han(fminInd:fmaxInd,j)=hanning(fmaxInd-fminInd
       +1);
end
dataShifted=dataShifted.*han;

%Bessel window for interpolation in cartesian space
at=10;
besselLength=100; %Must be larget than at
beta=pi*sqrt((besselLength/at)^2/(at^2)*(at-1/2)
   ^2-0.8);
besselWin=kaiser(besselLength,beta);

kSpace=zeros(2*size(dataShifted,1),2*size(
   dataShifted,1));

for Irow=1:size(kSpace,1) %for each k-space pixel
   row
    for Icol=1:size(kSpace,1) %for each k-space
       pixel column
        r=round(sqrt((Irow-size(kSpace,1)/2)^2+(Icol
           -size(kSpace,1)/2)^2)); %what radius does
            the pixel have
        if r>fminInd && r<fmaxInd
        a=atan2(Irow-size(kSpace,1)/2,Icol-size(
           kSpace,1)/2)+pi+pi/2; %what angle does
           the pixel have

        n=(size(dataShifted,2))*a/(2*pi)+1; %what
           index in data does the angle correspond
           to

          points=ceil(n-(besselLength-1)/(2*at)):
             floor(n+(besselLength-1)/(2*at)); %what
              data points to take into account
          besselp=round([fliplr(-rem(n,1)*at:-at:-(
             besselLength-1)/2) (1-rem(n,1))*at:at:(
             besselLength-1)/2]+(besselLength-1)
             /2+1); %where on the bessel function is
```

```
            each data point
        for p=1:length(points)
            if(points(p)<=0)
                points(p)=points(p)+size(dataShifted
                    ,2); %loop around if points go
                    below zero
            end

            if points(p)>size(dataShifted,2)
                points(p)=points(p)-size(dataShifted
                    ,2);
                                                    %
                    loop around if points go above max
                    angle
            end
        end

        values=sum(besselWin(besselp)'.*dataShifted(
            r,points)); %sum all weighted data points

        kSpace(Irow,Icol)=values; %add it to k-space
            pixel value
        end
    end
end

image=(abs(fftshift(ifft2(kSpace))));

dX=range(end)/size(kSpace,1);
XYscale=-size(kSpace,1)/2*dX:dX:size(kSpace,1)*dX/2-
    dX;
XYscale=XYscale*100; %in cm

maximg=max(max(db(image)));
imagest(XYscale, XYscale, db(image)-maximg,'Gridding
    (FFT)','cross-range (cm)', 'down-range (cm)');
caxis([-20 0]);
```

Printed by Tryckeriet i E-huset, Lund 2018

LUND
UNIVERSITY

Series of Master's theses
Department of Electrical and Information Technology
LU/LTH-EIT 2018-648
http://www.eit.lth.se